

Design Evolutions for Vortex Flow Control:  
Experimental Testing and Analysis of Modified Vortex Flow  
Control at Hydro-International plc.

I2 Individual Report

Project Supervisor: Dr Gavin Tabor

Eleanor Worrall

2010–2011

## **Abstract**

Stormwater management is under increasing strain with more severe weather patterns and growing demands for water. Here in the UK, conventional drainage networks do not have the capacity or robustness to accommodate frequent storm events, and downstream flood events throughout the country are on the rise. To combat this, Sustainable Drainage Systems (SDS) have been introduced to retain some of this excess stormwater at source and to attenuate its release into drainage networks. The Hydro-Brake® Vortex Flow Control (VFC) is a SDS device which acts a throttle within conventional drainage systems by inducing a vortex within the flow. This maintains a constant flow rate against the fluctuating water levels entering the network. This study looks at the current design of the VFC and proposes four options for modifying the design of its outlet in an attempt to further enhance the flow control capabilities of the device. Tests on performance and analysis against the current VFC characteristics are completed at Hydro-International plc. in their purpose built VFC testing facilities, and conclusions drawn on the impact of these modifications to the device operation. The results of these tests would suggest that the flow control capabilities of the VFC are heavily influenced by not only the Reynolds Number and Discharge Coefficients of the flow, but also the incircle area within the outlet. A reduction in this incircle area would appear to reduce the stability of the vortex induced, and hence the flow control capabilities of the VFC.

# Contents

<b>1</b>	<b>Project Overview</b>	<b>1</b>
1.1	Introduction . . . . .	1
1.2	Vortex Flow Control . . . . .	2
1.3	Project Aims . . . . .	4
1.4	Project Deliverables . . . . .	5
<b>2</b>	<b>Project Management</b>	<b>5</b>
<b>3</b>	<b>Relevant Literature and Related Studies</b>	<b>7</b>
3.1	A Study of the Design of Cylindrical Vortex Flow Controls for use in Urban Drainage Systems [15] . . . . .	7
3.2	Swirling Flow in a Fixed Container; Generation and Attenuation of a Vortex Column [20] . . . . .	9
3.3	Pressure Drop Across Vortex Diodes: Experiments and Guidelines [16] . . . . .	10
3.4	Transitional Process of a Swirling Vortex Generated in a Rotating Tank [14] . . . . .	10
3.5	Anatomy of a Bath Tub Vortex [2] . . . . .	11
<b>4</b>	<b>Ideas Development</b>	<b>12</b>
4.1	Test Rig and Experimental Planning . . . . .	12
4.2	Design Modifications . . . . .	12
4.3	Test Shapes . . . . .	14
4.4	Prototype Design . . . . .	14
<b>5</b>	<b>Relevant Theory</b>	<b>16</b>
5.1	Bernoulli's Principle and the Orifice Plate . . . . .	16
5.2	Low Flow Weir Equations . . . . .	18
5.3	Vortex Motion . . . . .	19
5.3.1	Free Vortex . . . . .	20
5.3.2	Forced Vortex . . . . .	21
5.4	Vortex Modelling . . . . .	22
5.5	Vortex Core Radius Approximation Models . . . . .	22
<b>6</b>	<b>Testing</b>	<b>24</b>
6.1	Experimental Facilities and Procedures . . . . .	24
6.2	Test Accuracy and Repeatability . . . . .	27
<b>7</b>	<b>Results</b>	<b>27</b>
7.1	Control VFC Tests . . . . .	28
7.2	Modified Outlet Shapes . . . . .	30
7.3	Low Flow Rates . . . . .	31
7.4	High Flow Rates . . . . .	32

7.5	Triangular Outlet Results . . . . .	33
7.6	Discharge Coefficient Results . . . . .	34
7.7	Theoretical Comparisons . . . . .	36
7.8	Vortex Core Radius . . . . .	38
<b>8</b>	<b>Conclusions</b>	<b>38</b>
8.1	Further Work . . . . .	39
<b>9</b>	<b>Acknowledgements</b>	<b>40</b>
<b>10</b>	<b>Bibliography</b>	<b>41</b>
<b>11</b>	<b>Appendix</b>	<b>43</b>

# 1 Project Overview

## 1.1 Introduction

There is no argument that climate change is happening; Whether this can be attributed to natural changes within the Earth's lifecycle or to an increase in Greenhouse Gas emissions as a result of human activity is however debatable. Nevertheless, a warmer climate has severe implications for global water management;

*Here in the UK, under the current 'High Emissions' climate change scenarios, precipitation in the 2080s in the South East would decrease by 50% in summer, and increase by up to 30% in winter, whereas in the North West, it may decrease by 30-40% in summer and increase by 20-25% in winter. [8]*

As a result, flash flooding is likely to become more frequent and more severe, coupled with increasing risks of drought and water scarcity problems.

Changing weather patterns are however not the only reason for the increase in flash flood events in the UK in recent years; with high levels of urbanisation through the expansion of cities and growing industrial developments, our natural environment is being compromised. This leads not only to a loss of vital habitats for wildlife, but a reduction in the volume of dense, highly permeable vegetation. The level of stormwater attenuation the natural drainage system provides into our drainage networks is therefore reducing. As a consequence, drainage networks are under greater strain from both more intense storm events, and increased rates of surface run-off. This increased intake of water is what often leads to downstream flooding, and for many areas of Great Britain, including parts of Cumbria and South Wales, surface water flooding is seen as a regular event.

The UK Government has recognised the urgent need for improved water demand management; however this is not a simple task. Conventional drainage networks convey all storm and waste water to treatment works from source as quickly as possible, and attempting to alter this vast network is a complex challenge. It would be impractical in many areas, due to space limitations within existing conventional drainage networks, to introduce sufficient upstream storage capacity or relief channels for these flood events. It would also be highly cost ineffective. Similarly, installing a range of smaller drainage pipes upstream to divert surface run-off would also be insufficient as these small pipes block easily from leaves and other debris.

Instead, Local Authorities are implementing sustainable drainage techniques to support conventional drainage networks throughout the UK.

*The aim of a sustainable drainage system (SDS) is to mimic the response of the existing catchment and its surfaces, ultimately with some betterment, negating any increased off-site flood risk that the development could cause,*

*i.e. Maintaining the surface water characteristics of the catchment to pre-development levels or better. [12]*

Alongside this, the Government has also recently introduced The Flood and Water Management Act 2010 [24] to remove the automatic right for new developments and redevelopments to connect to existing sewers. This forces developers to consider sustainable water management techniques and to ensure that as a result of their work, local flood risk will not increase.

## 1.2 Vortex Flow Control

The focus of SDS on sustainability highlights a need for drainage network adaptations that are not only effective at attenuating water passage, but which are simple to operate and easy to maintain. SDS devices therefore should cause no hindrance to the normal operation of the network, but be able to self-activate against flooding during storm events. SDS are commonly designed to maintain the passage of water through the system at a given maximum design level (usually predetermined by the Environment Agency [12] during periods of high rainfall whilst storing or diverting the excess rainfall. A particular SDS component this project focuses on is the Hydro-Brake® Vortex Flow Control (VFC). Hydro International Plc. have been developing and manufacturing flow control devices using advanced vortex technology for the last 25 years. The VFC functions very similarly to a vortex diode used in the nuclear industry; however VFCs are designed for stormwater purposes instead of nuclear fluids and allow flow to only pass in one direction (downstream). Vortex diodes permit flow in both directions. A VFC has no moving parts, and consists of an inlet, a conical chamber, and an outlet. The outlet faces downstream within the drainage network, and water enters the VFC inlet tangentially to the outlet pipe. VFCs are available in a variety of geometries, depending on their purpose and function. This project focuses specifically on the cylindrical-type VFC (see Figure 1 below), which has a square inlet and circular outlet.

The operation of a VFC utilises the phenomena of vorticity (see Section 3 for further details). Under low flow conditions, water can pass through the VFC with very little turbulence, the outlet acting as an orifice. This can be seen in Figure 2 below, where for low flow rates, head increases linearly with flow. As the VFC chamber fills, the pressure generated sets the water inside the chamber into helical motion. The upstream hydrostatic head of the VFC is transformed into kinetic energy. Only part of this kinetic energy is utilised as motion in the downstream direction, the greatest velocity component is perpendicular to the outlet [22]. With further increased inlet flow velocities, a transition from free flow to vortex flow occurs, inducing a vortex.

The point at which the vortex begins to initiate, labelled as Point B on Figure 2, is very near to the maximum design flow (Point A). This is advantageous as more water is able to pass through the VFC at the start of a storm event, reducing upstream water storage requirements [13].

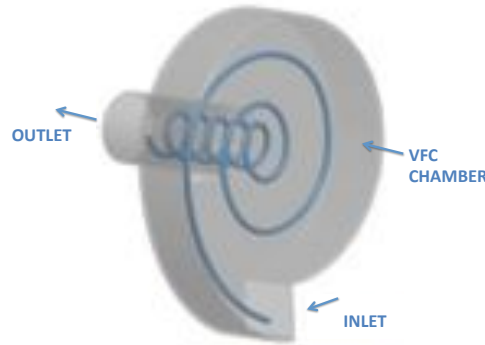


Figure 1: Diagram of cylindrical-type VFC [7]

At Point C, known as the kick-back, the vortex has fully initiated and head-flow characteristics return towards the desired design point (Point A). Flow is effectively choked, preventing excessive levels of discharge travelling through the drainage network, and a vortex is formed. The slight change in the graph labelled Point D indicates when the VFC is moving into a stable regime of vortex flow after the turbulent transition from free-flow to vortex flow. This transitional phase is the section of graph in Figure 2 between Points B and C, during which an air-filled core is formed within the flow. By Point C, all air has been expelled from the VFC chamber and the vortex stabilises [13].

Each size VFC has been specifically designed and tested to determine its maximum flow capabilities whilst in operation, as this flow rate depends on the physical dimensions of the unit and also on the differential head due to the flow rate and level of submersion of the device created. The Hydro International plc. website gives extensive details of the performance and design of the VFC [12].

Compared to a standard orifice within a drainage network VFC's therefore have many advantages;

1. A VFC can achieve the same discharge rates with a larger downstream opening. This can significantly reduce the risk of clogging within the network, and also allows river wildlife to pass through with greater ease than typical orifice openings or more traditional flow control devices
2. Discharge varies much less with water depth fluctuations in the storage basin through a VFC compared to a standard orifice, resulting in greater control and more constant flow release from the catchment
3. A VFC generates a significant reduction in the required upstream storage capacity as a result of increased flow control through the drainage network, generating significant construction costs

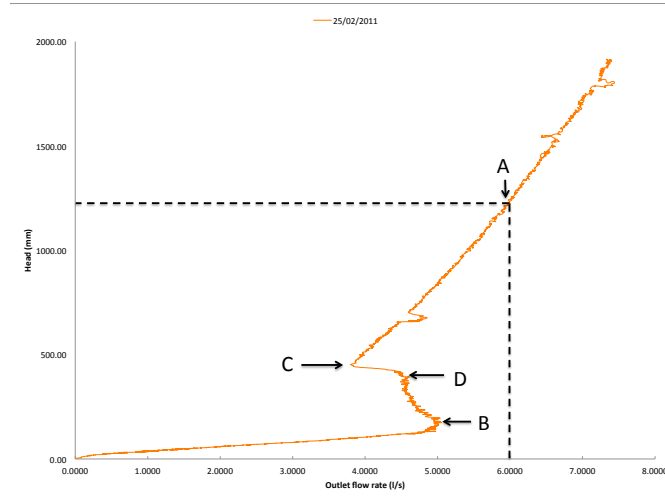


Figure 2: Head-flow characteristics of 100mm diameter cylindrical-type VFC with important operational features labelled [13]

### 1.3 Project Aims

Figure 3 gives a diagrammatic representation of the flow control capabilities of a VFC during a storm event. Whilst the VFCs flow control is more effective than a standard orifice plate, the main problem, which Figure 3 highlights, is that as the VFC transitions from free flow into vortex flow there are slight fluctuation within this control compared to the ideal outflow hydrograph response. The purpose of this project has therefore been to modify the current design of the VFC in an attempt to enhance its performance (achieve a control which more closely resembles the red line on Figure 3) during storm events. In other words, to maximise the flow rate through the VFC for all head levels, without exceeding the design flow rate.

The group project aims have therefore been

1. To understand the operation of a VFC
2. To generate appropriate design modifications (specifically for the cylindrical-type VFC shown in Figure 1)
3. To use Computational Fluid Dynamics (CFD) modelling and Experimental testing on a fully-functional prototype unit at Hydro-International, Clevedon UK to analyse the impact of these modifications on VFC performance
4. Create an in-house test rig at Exeter University to further analyse vortex flow regimes
5. Model the VFC within hydrology software InfoWorks CS and SWMM 5 to assess its flood risk reduction capabilities in a typical catchment area



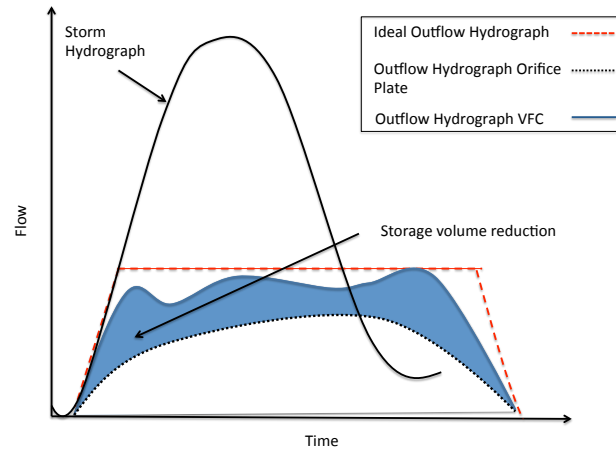


Figure 3: Graph demonstrating difference in Flow Control Capabilities of VFC against Orifice [12], [18]

## 1.4 Project Deliverables

Personal deliverables for this individual aspect of the project have included

1. Complete literature review of previous and related studies on vortex flow
2. Liaise with Hydro-International to arrange testing at Clevedon UK and ordering/collection of prototype VFC
3. Complete testing of modified VFC at Hydro-International, Clevedon UK
4. Analyse raw data from tests to establish impact on performance
5. Using relevant theory and related studies discuss whether these design changes have had desirable or undesirable effects on the VFC performance

## 2 Project Management

In Section 1.3 on page 4, key deliverables for this group project were clearly defined. To best manage these deliverables and to maintain awareness of individual progress against overall group progress, required areas of work were split into 'phases'. The relationship between these phases is provided in Figure 4, with more detailed descriptions in Table 1.

Alongside this Phasing Plan (Figure 4), other key management tools have included a Logbook and Gantt Chart. The use of a logbook proved very effective for project planning and for recording test information from Hydro-International. It has also formed

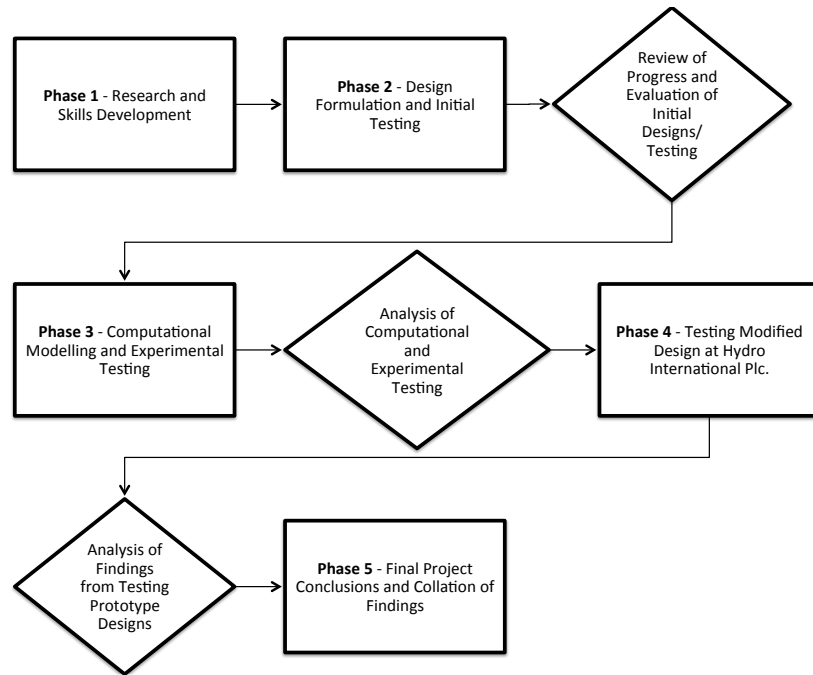


Figure 4: Flow diagram of project phasing

Table 1: Outline of project phases of work

Phase of Work	Description
Phase 1	Literature review, theoretical research and modelling, programming skill development including openFOAM, InfoWorks CS and SWMM 5
Phase 2	Manufacture of preliminary test rig and initial experimentation in fluids laboratory, construction of example meshes and unmodified VFC design meshes for analysis in openFOAM, analysis of drainage network case studies with VFC installed using InfoWorks CS/ SWMM 5
Phase 3	Full development of modified designs, introducing CFD to analyse effect on performance of VFC, full experimental investigations on vortex flow regime using in-house test rig, continuation of drainage network analysis using InfoWorks and SWMM 5
Phase 4	Manufacture of modified prototype VFC design and testing at Hydro International Plc. Phase 3 to continue within Phase 4
Phase 5	Report writing, conclusions of findings, evaluation of success of project, final presentation preparations

a useful record of personal progress throughout the project. Similarly, the use of a Gantt Chart presented the project plan very visually, and has been a valuable reference for monitoring progress and checking-off deliverables. The project Gantt Chart is attached

in the report Appendix (Section 11) on page 44.

Overall, project progress remained on schedule and according to Figure 19. Testing was started a few days later than forecasted, but took a shorter time to complete, therefore finishing exactly to time. Certain aspects of Figure 19 initially forecast were managed by other group members, particularly the in-house test apparatus construction (Phase 2) and in-house testing (Phase 3). These aspects have however remained on Figure 19 as many of the key deliverables outlined in Section 1.3 on page 4 were dependent upon these areas of works being successfully completed.

### 3 Relevant Literature and Related Studies

#### 3.1 A Study of the Design of Cylindrical Vortex Flow Controls for use in Urban Drainage Systems [15]

In this work, [15] completed an extensive study into the hydraulic behaviour of confined swirling flows with particular focus on the cylindrical-VFC case. The authors aim was to further understand the fluid mechanics of this VFC in order to develop theoretical models and design procedures that maximised its storage saving capacity for a given urban drainage scenario. The four operational modes described in Figure 5 and Table 2 were observed during this investigation, and provide a useful insight into flow behaviour within a cylindrical-type VFC.

The concept of swirling flow (Mode 2) described by [15] is based on a relationship first proposed by [10]. In this relationship, Swirl ( $S$ ) is quantified by the dimensionless ratio of the axial flux of the swirl momentum ( $G_\theta$ ) divided by the product of the axial flux (of the axial momentum) ( $G_z$ ) and swirl radius ( $r$ )

$$S = \frac{G_\theta}{G_z r}$$

$$G_\theta = 2\pi \int_0^\infty \rho U_\theta U_z r^2 dr$$

$$G_z = 2\pi \int_0^\infty \rho U_z^2 r dr + 2\pi \int_0^\infty p r dr$$

By neglecting  $2\pi \int_0^\infty p r dr$ , the Swirl Parameter  $S_g$  can be defined based on the geometry of the unit and the mean flow conditions [15]

$$S_g = \frac{\pi r_c r_o}{A_t} \quad (1)$$

Where  $r_c$  = the chamber radius,  $r_o$  = the outlet radius and  $A_t$  = the inlet area.

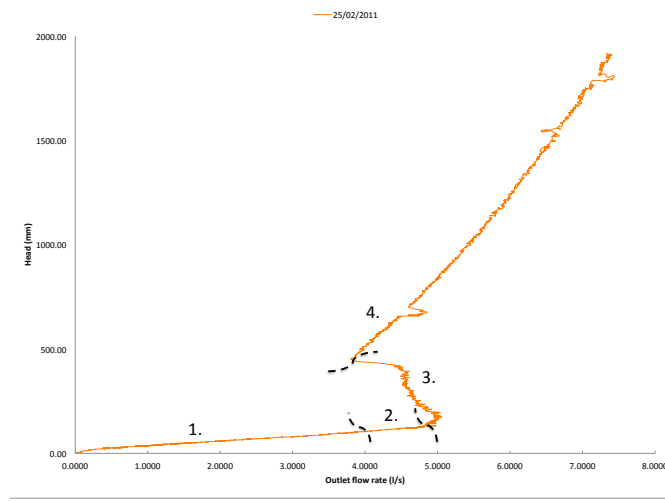


Figure 5: Head-flow graph of VFC with 100mm outlet diameter demonstrating flow regime changes during operation [15]

Table 2: Description of flow regimes within a cylindrical-type VFC at different flow rates

Mode	Internal VFC Water Level	Flow Description
1.	Water level below top edge of outlet pipe	Gravity-driven; VFC acting as an orifice
2.	Water level above top edge of outlet pipe	Swirling flow induced, no vortex or vortex core present
3.	Further increase in flow causes rapid increase in upstream head but negligible change in flow (refer to Figure 5)	Transition between swirling flow and vortex flow occurring; air core formed as flow rate increases and becomes more turbulent
4.	Chamber full of water	Vortex stabilised and continuing, air fully expelled from VFC chamber

Further in [15], the author directly measured pressure and velocity distributions across the VFC, using pressure tappings, on a 100mm diameter outlet cylindrical-type VFC to gauge the diameter of the vortex air core formed during Mode 3 (Table 2). To investigate this in more detail, using CFD, [15] found the pressure contours across the axial mid-plane of the VFC clearly demonstrated precession of the vortex core for different flow-volume exchange periods [15]. The author found that the core radius could exist between 55% and 96% of the outlet radius depending on the flow rate induced.

Through the experimentation completed as part of this study at Hyro-International, Clevedon the author also found hysteresis within the formation and collapse of the vortex core. This significantly effected the hydraulic behaviour in the transitional zone (Mode 3) of the VFC between tests, however the other operating modes were unaffected. This could have significant impact on the performance of a VFC during storm events, and is important to remain aware of in this study.

### **3.2 Swirling Flow in a Fixed Container; Generation and Attenuation of a Vortex Column [20]**

The experimentation demonstrated in this study is at a level much higher than that achievable within the time scale and facilities available for this project. A two-dimensional Particle Image Velocimetry (PIV) system and dye tracking techniques are successfully employed on a vortex within a fixed container. This study therefore aims to utilise these techniques for the in-house vortex experiments, although at a more basic level.

The focus of [20] is specifically on the strong connection between the bottom boundary layer of the fluid and the formation of a vortex. It is concluded by [20] that the vortex strength for a given flow rate can be controlled by the thickness of this bottom boundary layer. Whilst [20] realise the complexity of theoretically modelling the formation of a vortex, due to the combination of an array of flow regimes and instabilities, the paper also presents a simplified theoretical model for the formation of a vortex. This is applied to a select range of the flow regimes analysed within their investigations.

The experimental procedures implemented two independent hydraulic circuits of flow, one inducing circulation and the other suction, so that fluid height within the test rig remained constant. This increased the accuracy to which the time dependent variables, such as flow rate, of the resultant flows could be analysed. The flow produced due to firstly each of these circuits acting independently, and then with various ratios of both flows combined, was analysed using PIV. PIV enabled [20] to assess the velocity fields at different heights within the column of fluid, and dye injection enabled the flow behaviour to be observed with greater clarity.

With only circulation flow input to the base of the fluid column, [20] found that the tangential velocity of the flow could be established entirely analytically providing the inlet flow rate was controlled accurately and that it remained a known parameter. Once a small level of suction flow was added into the circulation flow, [20] concludes that the average velocity profile approaches that of a rigid rotation; with greater levels of suction introduced, there forms a columnar vortex, the intensity of which increases with the suction flow rate applied.

### 3.3 Pressure Drop Across Vortex Diodes: Experiments and Guidelines [16]

A vortex diode is a non-return valve implemented in the nuclear power industry. As mentioned in Section 1.2 on page 2, these devices are similar in function to a VFC. Diodicity describes the performance of a vortex diode, and is the

*ratio of pressure drop for reverse (the undesired flow direction) and forward flow (desired flow direction) for the same flow rate [16]*

The diodicity within a vortex diode should therefore be as high as possible in order for it to operate with the highest efficiency. As the authors continue to explain, tangential inflow is found to be crucial to the formation of a vortex; the strength of this formed vortex is dependent upon both the tangential inlet flow rate and the geometry of the chamber where the vortex is induced. For a confined vortex such as that within a vortex diode (and thus a VFC), according to [16] tangential flow within the chamber is clearly divisible into two zones:

1. Region of constant circulation (free vortex zone)
2. Forced vortex zone

The challenge designers and researchers therefore face for vortex diodes is understanding (and predicting) where the transition between these two vortex zones arises. To mathematically model the vast array of flow regimes and deformations occurring simultaneously within the flow is also a highly complex proposition. Add in the influence of unit geometry to these flow regimes, and the problem is further enhanced. What [16] do conclude however is that the stability of the vortex is directly related to its strength; with higher flow rates, vortical flow is stronger, but again, this is not infinitely true as the geometry of the unit has an influence on the vortex formation.

Following from this, it is also noted that a large vortex diode will yield a higher diodicity, and interestingly, [16] report that with the inlet pipe, vortex chamber and outlet pipe all at a constant diameter, higher diodicity was found. Alongside this, [16] also mention that the symmetry of the vortex diode was found to have an influence on its performance; In asymmetric designs, the vortex centre may oscillate close to the exit of the chamber, reducing the stability of the vortex.

### 3.4 Transitional Process of a Swirling Vortex Generated in a Rotating Tank [14]

In-depth experimental investigations on vortical flows are carried out in this study, providing a good insight into the transitional phases that occur within fluid flow in order for a vortex to be induced. These transitional changes are examined in a rotating tank, using a syphoning mechanism to firstly initiate the vortex. PIV and dye injection techniques are then implemented to monitor flow.

In summary, the formation of a contained vortex such as this is described by [14] in three stages; firstly, a siphoning stage is required to induce tangential velocity. Immediately after the removal of this siphon, the pressure difference created causes a downward jet with an air core to form from the free surface of the vortex. This runs through the entire vortex depth down to the bottom boundary layer, and this is known as stage two.

This air core draws in water from the free surface of the vortex, again due to the pressure differences created, causing the water to flow downwards through the core toward the outlet pipe. An "inner vortex" develops, whilst the remainder of the fluid in the container is still relatively stable, spiralling much more slowly upwards around this inner vortex [14]. As the flow continues to develop, eventually the inner vortex cell begins to detach from the bottom of the tank. As a result, the very bottom boundary layer of fluid in the tank spirals upwards, effectively against the downward jet, creating a small 'cup-like' region observed around the outlet pipe of rotating fluid. The concept of studying the transition of a vortex like this is complex, and [14] were some of the first to achieve results for this type of "two-celled" vortex analysis.

### 3.5 Anatomy of a Bath Tub Vortex [2]

An overview of the common Bathtub vortex, observed as water empties through a plug-hole is provided in this study. This vortex is described by the authors as

*a result of strong, localised deformations of free surfaces.*

This study looks at a stationary vortex within a rotating container, which drains through a small outlet pipe under gravity. With increased angular velocity of the container, it was found that a greater surface depression occurred at the top surface above the centre of rotation. The depth of the surface depression increased to a point, above which, the tip lost stability and bubble shedding occurred; a process in which air bubbles from the flow are forced onto the tip of the surface depression and down the outlet pipe. This was noted by other previous literature as the core of the vortex through the middle of the flow of water.

Through the application of two very fine streams of fluorescent dye; one at the surface of the vortex and the other at the very bottom, it was shown that at the top of the vortex, a distinct, highly concentrated line of dye was produced. Contrastingly, a scattered spiral of dye was produced at the bottom of the vortex. This would suggest flow is strongly localised around the surface tip of the vortex, and water from a thin surface layer travels towards the vortex core, where it is then diverted downwards and through the outlet pipe. Interestingly, only a small fraction of the flow through the plughole was observed to have originated from the surface region directly above the outlet pipe.

It is therefore proposed by [2] that nearly all flow is provided to the outlet by the thin Ekman layer in the bottom of the container. In this boundary layer, fluid was observed to spiral inwards towards the drainage hole. Once the fluid had arrived near the plughole,

it was directed upwards, effectively around the rapidly rotating vortex core described above, and then down the plughole with the rest of the flow. The fluid in the rest of the container is very undisturbed and as [2] note, can effectively be modelled in a 2D system for simplification of calculations. This links with the findings of [14] and the concept of a two-cell vortex regime.

In conclusion, the study speculates a critical value for the angular velocity at which bubble shedding is induced. This links to the concept of downwards drag on the fluid being sufficient to overcome the buoyancy forces acting within the fluid, and therefore drag both the bubbles and the fluid down through the plug hole.

## 4 Ideas Development

### 4.1 Test Rig and Experimental Planning

As the previous studies have highlighted, in particular [20], PIV and dye injection techniques are effective methods of exploring flow velocity fields within a fixed container vortex. For the in-house experimentation within this project, the design of the test rig was therefore centred around the implementation of PIV. It was decided that due to the precision required to successfully employ dye injection techniques this would not be feasible within the laboratory facilities and project budget. Further to this, a common conclusion throughout all the previous studies in Section 3 is the concept of a *two-cell vortex*. As the literature describes, this is the phenomena of an air-core filled vortex surrounded by a free-vortex regime. These studies have therefore also provided some key ideas about the formation of a forced vortex and its behaviour to take forward into the experimental stage of the project.

To best plan the experimental phase of the project, an initial visit to Clevedon, where Hydro-Internationals offices are based here in the UK, was scheduled. This provided the opportunity to gain an understanding of the capabilities of the test facilities, and to also speak with members of the Research and Development Department about potential modification ideas.

### 4.2 Design Modifications

In order to maintain control and accuracy within both the experimental and computational modelling aspects of the project, only one feature of the VFC was selected for modification. As discussed with our Project Supervisor and a Hydro International Plc. representative, Daniel Jarman, a large number of geometric features within the VFC design could be altered to tailor its hydraulic characteristics, including;

- Outlet pipe to chamber diameter ratio



Axial length of chamber  
 Inlet area and/or outlet area  
 Outlet and/or inlet shape  
 Position of Inlet/Outlet  
 Number of Inlets/Outlets  
 Shape of chamber axial cross-section  
 Inserts/vanes inside the flow chamber

As a group it was decided to focus our design modification on the VFC outlet shape. Although this modification is quite straight forward with respect to unit design changes, it may have a significant impact on the performance of the VFC. From literature, [16] suggest that an asymmetric design has a considerable impact on the stability of the vortex induced. Referring back to Figure 3, these tests may therefore establish whether changing this vortex stability enables greater or reduced flow control within the VFC. What is therefore hoped to establish within this investigation is whether a more constricting outlet shape chokes the flow further, increasing the flow-control capabilities of the VFC, or whether it disrupts the vortex formation in a negative way, permitting greater volumes of flow with increasing head through the device.

Further to this, changing the outlet shape is a modification Hydro-International Plc. have never investigated within their Research and Development to date. It is therefore of interest to the company, and an entirely new area of experimentation. In addition, if found to have any positive effects on the performance of the VFC, changing the outlet shape would not be too costly for Hydro-International to implement within the design and production of their cylindrical-type VFCs.

Another benefit from this design modification is that it can also be incorporated within the in-house experiments at Exeter University on the characteristics of vortex flow with relative ease. This provides the opportunity to also explore the changes to vortex flow under the influence of a non-circular cross-sectional outlet pipe. Adapting theoretical modelling at low flow rates in line with this modification should also be feasible. CFD modelling adaptations should also be accurately achievable within this design adjustment.

It was also felt that given the short time to complete this project, any complex design alternations, for example installing inserts within the flow chamber, would require a long lead-time for manufacture of the prototype unit. This would also create unaffordable cost implications for the group.

Further still and referring back to Equation (1)

$$S_g = \frac{\pi r_c r_o}{A_t}$$

It can be seen that this swirl parameter is directly influenced by the outlet radius, chamber radius and inlet area. If these ratios were to be altered, a second variable would be introduced to the tests as the swirl parameter could be subject change. For this reason and to focus on the impact of only one variable of the VFC design, it has been decided to maintain the inlet to outlet ratio within the shape modifications implemented. All outlet shapes will therefore have the same cross-sectional area as the circular outlet on the standard 100mm diameter cylindrical-type VFC.

### 4.3 Test Shapes


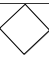


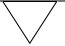

There were a range of possible outlet shapes considered for testing. Again due to the time limits on the project and the considerable length of time required to complete each test, five options were prioritised with a sixth test arranged for a control unit. A square and triangle were selected as the most suitable shapes to test because they provide good variety against the standard circular outlet, but also can be rotated into two other orientations. This not only generates cost savings from reduced prototype manufacturing requirements, but these alternative orientations may produce considerable differences in the VFC performance. Importantly, these two shapes are the more realistic options for alternative outlet shapes, as complex shapes could increase problems for blockages within the VFC from stormwater debris.

### 4.4 Prototype Design

An image of the prototype device can be seen in Figure 6 below. The unit was specifically designed with an inter-changeable outlet plate, attachable and detachable by a series of bolts through an external flange. This was to allow each of our modified shapes to be tested on the same VFC unit and in a variety of orientations. Three test plates were therefore manufactured, a square, triangular and circular plate, as detailed in Table 3. The purpose of manufacturing and testing a circular plate, as again Table 3 highlights, identical in size to the unmodified cylindrical-type VFC unit was for comparative purposes between the standard unit and the prototype unit.

The VFC was manufactured using the same materials and techniques as the VFCs installed in drainage networks. Manufactured from grade 304 stainless steel, this was cut using Computer Numerical Control (CNC) techniques to an accuracy of  $\pm 0.3\text{mm}$  [15]. The heat generated from the cutting and welding processes used in the manufacturing processes may have caused the VFC unit to warp very slightly, but to no hinderance of the tests and in line with the distortions which would be present in all VFCs manufactured by Hydro-International. The technical drawings for this prototype unit can be found in the Appendix in Section 11.

Table 3: Selected modified VFC outlet shapes and design descriptions

Order	Test Name	Outlet Shape	Dimensions (as drawn)	Description
1.	Control		100 mm Diameter	Unmodified Cylindrical-Type VFC
2.	45° Square		90mm	Diamond orientation with points perpendicular to VFC chamber
3.	Square		90mm	Flat bottom (parallel to bottom on VFC) square outlet
4.	Circle		100mm Diameter	Identical outlet to standard Cylindrical-Type VFC but tested using prototype unit for results redundancy
5.	30° Triangle		134.6mm (equal sides)	Triangle with point vertically down towards base of VFC chamber
6.	Triangle		134.6mm (equal sides)	Triangle with flat base

Note: 30\_deg Triangle and 45\_deg Square  $\equiv$  to 30 ° Triangle and 45 ° Square on all graphs in Section 7

Actual measured dimensions for the VFC prototype unit and the interchangeable plates are listed in Table 4 below. As the figures in Table 4 demonstrates, whilst the drawings were designed to maintain a constant outlet area across all three outlet shapes, there is a discrepancy of approximately 16.1 mm<sup>2</sup> in the VFC outlet areas between the three manufactured plates. This difference in area is negligible and reasonable to attribute to manufacturing tolerances. This discrepancy is not significant enough to cause any concern of the accuracy of the tests or to realistically question the continuity of the outlet areas between each of the test plates.

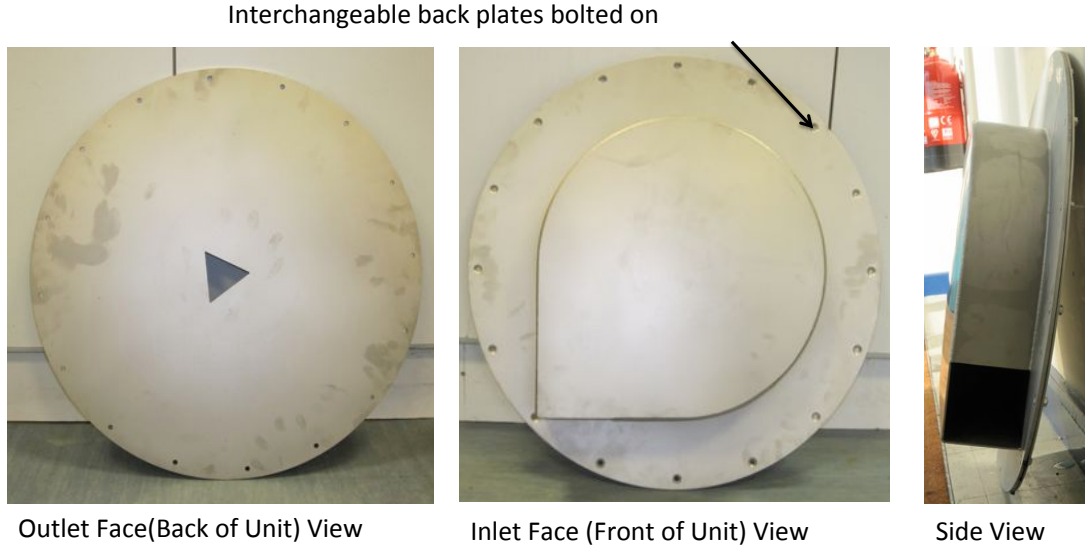


Figure 6: Images of the prototype VFC with interchangeable back plate

Table 4: Measured dimensions of prototype VFC unit and interchangeable plates

Dimension	As drawn (mm)	Actual (mm)	C-S A (mm <sup>2</sup> )
VFC Chamber Radius	197	195	N/A
VFC Unit Diameter	610	612	N/A
VFC Inlet	100 x 100	100.7 x 100.3	10100.2
VFC Flange Thickness	5	5.2	N/A
VFC Unit Thickness	3	3.3	N/A
Square Plate	88.620	89	7921.0
Circular Plate	100	100.5	7932.7
Triangular Plate	135.4 (sides)	135.1 (sides) 117.5 (height)	7937.1

## 5 Relevant Theory

### 5.1 Bernoulli's Principle and the Orifice Plate

According to [6] Bernoulli's Principle States that for an assumed frictionless, steady state, laminar and incompressible flow, an increase in velocity of flow occurs simultaneously with a decrease in the fluid pressure. This relates to the Principle of Conservation of Energy where the sum of the kinetic energy and potential energy along a streamline must remain constant within a closed system. The total head (H) within a system can therefore be described as

$$H = z + \frac{P}{\rho g} + \frac{v^2}{2g} \quad (2)$$

Thus between two points

$$\frac{P_1}{\rho g} + \frac{v_1^2}{2g} + z_1 = \frac{P_2}{\rho g} + \frac{v_2^2}{2g} + z_2 \quad (3)$$

P = pressure at point (point 1 or 2 respectively),  $\rho$  = density of water, g = gravitational constant, z = hydraulic head at point and v = velocity of flow at point.

An orifice plate is a useful and highly accurate device for measuring flow rate that implements the Bernoulli principle. Typically VFCs are installed in drainage networks within pipes of diameters much greater than the outlet hole size of the VFC, therefore flow is forced to converge through the VFC in the same way as an orifice plate. This creates a change in velocity, and therefore a corresponding pressure difference across the VFC. Downstream of the orifice plate, flow area expands instantaneously, whilst the fluid is unable to expand at the same rate [5]. The result is a separation zone of turbulent eddies in which large energy losses occur. The coefficient of discharge ( $C_d$ ) is therefore introduced to account for these energy losses within flow rate calculations for orifice plates. By applying Bernoulli's principle between a point in the flow a small distance downstream of the outlet (where streamlines are considered straight and parallel) and the water surface (where pressure is atmospheric),

$$\begin{aligned} \frac{P_0}{\rho g} + h &= \frac{P_0}{\rho g} + \frac{v^2}{2g} \\ v &= \sqrt{2gh} \end{aligned} \quad (4)$$

Since

$$\begin{aligned} Q &= vA \\ Q_{ideal} &= A\sqrt{2gh} \end{aligned} \quad (5)$$

Where A = the area of the jet, which is smaller than the area of the orifice due to the convergence of streamlines [5]. Equation (5) originates from the work of Torricelli [5]. The jet contraction is called the *vena contracta* and experiments have shown jet area (A) and orifice area ( $A_0$ ) to related by

$$A = C_c A_0$$

Where ( $C_c$ ) = the coefficient of contraction.

In addition, energy losses are incurred at the orifice itself, therefore another coefficient is introduced to account for these, the coefficient of velocity ( $C_v$ ), giving

$$\begin{aligned} Q_{actual} &= C_v C_c A_0 \sqrt{2gh} \\ Q_{actual} &= C_d A_0 \sqrt{2gh} \end{aligned} \quad (6)$$

Discharge Coefficient ( $C_d$ ) =  $C_c \times C_v$

$Q_{actual}$  = the outlet flow rate from the orifice plate (or out of the VFC in the case of this study).

## 5.2 Low Flow Weir Equations

At low flow rates, whilst the VFC is not full of water and swirling flow is yet to be induced (Mode 1 Table 2), the outlets act as a weir. The triangle and square outlet orientations can be treated as a contracted rectangular weir, whilst both the 30° triangle and 45° deg square are representative of a vee wier. As [5] describes, particularly at low flow rates, compared to rectangular weirs, vee weirs are considered more accurate flow measuring devices. This is due to the greater increase in upstream head with a given increase in flow rate, and therefore greater sensitivity over which the vee weir operates. However, this greater sensitivity of the vee weir does limit the range of discharge over which the weir can be applied economically [5].

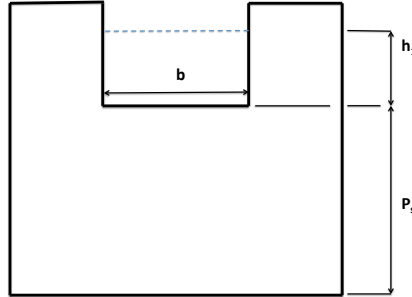


Figure 7: Cross-sectional view of rectangular weir [5]

$P_s$  = the height of the weir crest,  $b$  = width of flow and  $h_1$  = depth of water above weir in Figure 7. For the case of the rectangular weir in Figure 7, according to [5] ideal flow over the weir can be calculated by the following expression

$$Q_{ideal} = \frac{2}{3} b \sqrt{2gh_1^{\frac{3}{2}}} \quad (7)$$

This theoretical value for  $Q_{ideal}$  from [5] varies from the actual discharge,  $Q$ , achievable over the weir due to

1. Convergence of streamlines in the flow at the weir
2. Actual pressure distribution in the flow passing over the weir is non-atmospheric
3. Energy losses and a non-uniform velocity distribution in the flow channel occurring due to viscous effects within the fluid

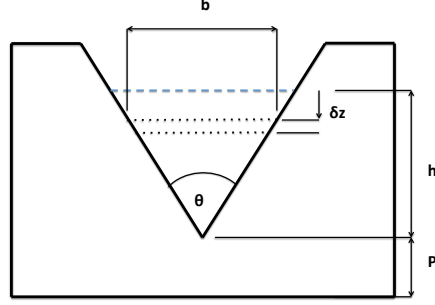


Figure 8: Cross-sectional view of vee weir [5]

$\delta z$  = elementary strip of discharge over wier.

For the Vee Weir case (Figure 8) theoretical assumptions for the rectangular weir remain valid [5], but  $b$  is no longer a constant, rather a function of the depth of water from the base of the weir ( $h_1$ ) therefore,

$$Q_{ideal} = \frac{8}{15} \sqrt{2g \tan \frac{\theta}{2}} h_1^{\frac{5}{2}} \quad (8)$$

### 5.3 Vortex Motion

As much of the literature on previous studies has highlighted, vortex motion is highly complex, and consists of a multitude of different interacting flow regimes. As [6] describes, flow is circular within a vortex, therefore flow velocity undergoes a continuous rate of change. This acceleration is the result of a force acting on the fluid, as Newtons Second Law states that

$$Force = mass \times acceleration \quad (9)$$

This force is due to the pressure differences created between adjacent streamlines; each streamline has a different radius, and since the pressure is lower closer to the centre of the vortex (because the streamlines have a smaller radius in this region) this force acts radially across the streamlines and they are accelerated towards the centre of curvature.

The combination of changing pressure head in a radial direction and changing velocity head from one streamline to another are responsible for the circular motion observed with no external source of energy [5]. For any flow with circumferential streamlines and assuming they remain in a horizontal plane (there is no change in potential head), then the change in total Head (H) with radius (r) can be calculated as follows

$$\frac{dH}{dr} = \frac{v}{g} \left( \frac{v}{r} + \frac{dv}{dr} \right) \quad (10)$$

Where  $\left(\frac{v}{r} + \frac{dv}{dr}\right)$  is the vorticity of the flow,  $g$  = Gravitational constant and  $v$  = velocity of fluid

### 5.3.1 Free Vortex

A free vortex is often observed after removing a plug from a bath and allowing the water to drain naturally through the plughole. It is described as a "free" vortex simply because there is no input energy from an external source. The streamlines of this vortex are assumed concentric, and since there cannot be any flow across streamlines, the flow is confined purely to circular paths; in other words, the radial component of velocity is zero. In [6], the authors explain that Equation (10) is valid for most vortex flows, but in the specific case of a free vortex the variation of velocity with radius is such that

$$\begin{aligned} \frac{dH}{dr} &= 0 \\ \frac{v}{g} \left( \frac{v}{r} + \frac{dv}{dr} \right) &= 0 \\ \frac{dv}{v} + \frac{dr}{r} &= 0 \\ \int \frac{dv}{v} + \frac{dr}{r} &= \ln v + \ln r + C \\ vr &= C \end{aligned}$$

Where  $C$  is the strength of the vortex and is a constant at radius  $r$

Using Equation (2)

$$H = z + \frac{P}{\rho g} + \frac{v^2}{2g} = \text{constant at any point}$$

For any point within a free vortex

$$H = z + \frac{P}{\rho g} + \frac{C^2}{2gr^2} = \text{constant at any point}$$



This therefore implies that as the radius of a free vortex tends to zero, the velocity of the vortex towards the central core tends to infinity. In other words, the tangential velocity varies inversely to the distance (radius  $r$ ) from its centre of rotation.

### 5.3.2 Forced Vortex

Similarly, [6] explains within a forced vortex, the fluid rotates as a solid body at a constant angular velocity,  $\omega$ . At any radius ( $r$ ) velocity ( $v$ ) is equal to angular velocity ( $\omega$ ) multiplied by this radial distance from the centre of the vortex

$$v = \omega \times r$$

Where  $\frac{du}{dr} = \omega$

From Equation (10)

$$\begin{aligned}\frac{dh}{dr} &= \frac{\omega r}{g} \times [(\omega + \omega)] \\ &= 2 \left[ \omega^2 \times \left( \frac{r}{g} \right) \right]\end{aligned}$$

$$\begin{aligned}\int \frac{dh}{dr} &= 2 \left[ \omega^2 \times \left( \frac{r}{g} \right) \right] \\ H &= \left[ \omega^2 \times \left( \frac{r}{g} \right) \right] + C\end{aligned}\tag{11}$$

Where  $C$  = constant of integration. For any point in the fluid, substituting in Equation (2) for  $v$  from Equation (11) gives

$$\begin{aligned}z + \frac{P}{\rho g} + \frac{v^2}{2g} &= \left[ \omega^2 \times \left( \frac{r}{g} \right) \right] + C \\ H &= \frac{P}{\rho g} + \frac{\omega^2 r^2}{2g} + z\end{aligned}\tag{12}$$

Therefore equating Equations (10) and (11)

$$\frac{P}{\rho g} + z = \frac{\omega^2 r^2}{2g} + C\tag{13}$$

Whilst these relationships and equations for vortex flow may not be directly applicable to the results of this study, it is useful to understand the mechanisms of these vortex types to understand any changes in vortex flow that may be observed during these VFC experiments.

## 5.4 Vortex Modelling

Since previous literature has suggested altering the outlet shape could have considerable impact on the formation of a vortex within the VFC [16], it is worth considering relevant models which describe how this vortex is formed and how it behaves. It should firstly be noted that in a real fluid, it is not possible for a free or forced vortex to prevail due to the viscous effects present in the fluid [6]. What many authors have therefore previously struggled to predict is the transition between a free and forced vortex within fluid flow. Many have however successfully modelled fluid flow between these two vortex regimes.

The *Rankine Vortex* [1] is considered one of the simplest vortex models available, treating a columnar vortex, such as that induced within a VFC, as a cylinder vortex with a finite core and constant vorticity. Surrounding this core, flow is assumed to be irrotational. Viscous effects within the vortex core of the fluid are also neglected [1]. The Burgers Vortex [4] is a more advanced model stemming from the Rankine Vortex in which

*the vorticity distribution and azimuthal velocity for a three-dimensional steady-state vortex [1]*

are expressed as solutions of the Navier-Stokes equations. The Burgers vortex assumes vortical flow to be bounded within a rotating porous tube of infinite length, with proper boundary conditions defined at the container walls [1]. This model can therefore be considered representative of a one-celled vortex, in which only vortices with positive axial velocities exist [15].

A more progressive solution from the Burgers Vortex which is of particular interest for this study is that established by Sullivan [23]. Sullivan obtained an exact solution to the Navier-Stokes equations in the form of a steady two-celled vortex [1], meaning that reversed axial flow was accounted for within the vortex core as well as in the flow surrounding the core. This model provides a very good representation of swirling flows in a boundless space, and the vortex core can be observed as a re-circulation region within this vortex core.

## 5.5 Vortex Core Radius Approximation Models

In [3], studies were completed on the behaviour of whirlpools. The authors found that with tangential inlet flow only, critical results for Head and Flow Rate achieved were much lower than those found with an entirely radial inlet flow. This was attributed

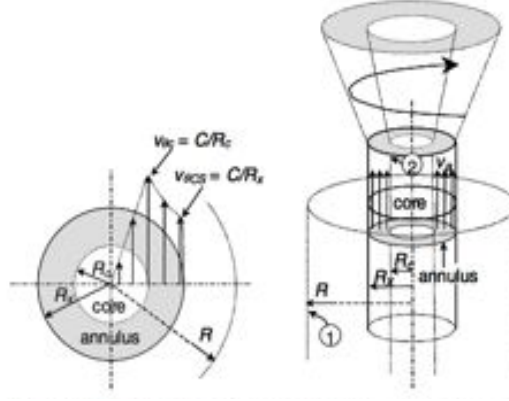


Figure 9: Plan (left) and elevation (right) views of the tangential and axial velocity profiles within the vortex tube for the stagnant-core flow model [11] (p73)

largely to the permanent air-core induced through the pipe as a result of the swirling flow. This air-core thus reduced the the cross-section of pipe available for water flow [3]. Another factor was also the large tangential component of velocity in the horizontal plane, which diminished the desirable vertical component of velocity. By combining radial and tangential supplies, [3] found that greater discharge was associated with a coreless flow. At very low heads however, the effect of swirl upon the discharge was negligible [3]. Within their findings were attempts to define the vortex core radius [3]. The authors observed downwards (towards the outlet of the test trumpet) motion of air through the flow purely due to surface friction within the fluid. This work was therefore one of the first to model a vortex in two-cells; a core solid-body of rotational flow with negligible axial velocity surrounded by a region of potential vortex flow with a uniform axial velocity [11].

More recently, in a study by [11], a *Core Flow Model* was defined for computing the loss in static pressure in a vortex tube, as opposed to the permanent frictional presses loss, in a similar manner to [3]. The authors of [11] measured dynamic pressure in the vortex finder based on the maximum swirl velocity at the inner edge of the core of the vortex. Of particular importance is the conclusion that both axial and tangential velocity components contribute to the static pressure drop across the vortex tube, and that these can be defined by pressure loss coefficients which can be defined in terms of the vortex core radius ( $R_{cx}$ ) [11].

From this, [11] continue to define the core radius, ( $R_c$ ) by assuming that, for given values of the tangential velocity ( $v_{\theta CS}$ ) at  $R_c$ , and the average velocity measured at the outlet of the vortex tube ( $v_x$ ), the vortex core radius will adjust so that the static pressure loss is minimum. In other words [11],

*the core radius will adjust to maximise flow at a given pressure difference.*

Equation (4.3.14) from [11] summarises this;

$$v_{\theta CS}^2 = \frac{2R_{cx}^4}{(1 - R_{cx}^2)^3} v_x^2 \quad (14)$$

The authors of [11] demonstrate from Equation 14 that as the core radius approaches the limiting value of one, the tangential-to-inlet ratio increases without limit. This implies that a design characterised by intense spin will result in flow exiting the vortex tube via a thin annulus near the wall of the vortex tube [11]. As the core radius approaches the other limiting value of zero, the tangential-to-axial ratio disappears. This suggests a design with only very weak spin will result in predominately axial flow filling the cross-sectional area of the vortex tube.

It was found by [11] that a very good approximation for the vortex core radius ( $R_{cx}$ ) could be given by the following Equation (Equation 4.3.15 in [11])

$$R_{cx} = \frac{0.0219 (v_{\theta CS}/v_x)^{-0.686} + 1}{0.700 (v_{\theta CS}/v_x)^{-0.686} + 1} \quad (15)$$

It should be noted that Equation 15 does not account for any pressure losses that occur at the entrance of the vortex tube [11]. Whilst it may not be in the scope of this project to analyse the VFC vortex core in such detail as the authors of this book, the findings of [11] could be highly useful for explaining any result variations established here.

## 6 Testing

### 6.1 Experimental Facilities and Procedures

The test facilities owned by Hydro-International Plc, at their Clevedon offices are purpose built for testing VFCs and for analysing hydraulic characteristics such as head and flow rate through the units. The test facilities were fully operational thanks to the previous work of [17], [18] and [15]. Extensive details of the test facilities and equipment specifications can be found in [15].

The facilities consists of a series of seven tanks in a re-circulating pumped (Pumpex - P3001V semi-submersible pump) system. The system extends over two floors of the building, pumping water from the ground floor sump tanks up into the three test tanks on the first floor. Flow returns to the sump tanks via gravity. Adjusting the frequency of the pump via an inverter controls flow through the system, therefore both measured head and measured flow rate are dependent variables of the tests.

The image in Figure 10 shows the test tank orientations on the first floor of the building. Connected to the test facilities are two pressure transducers, one at the inlet of the

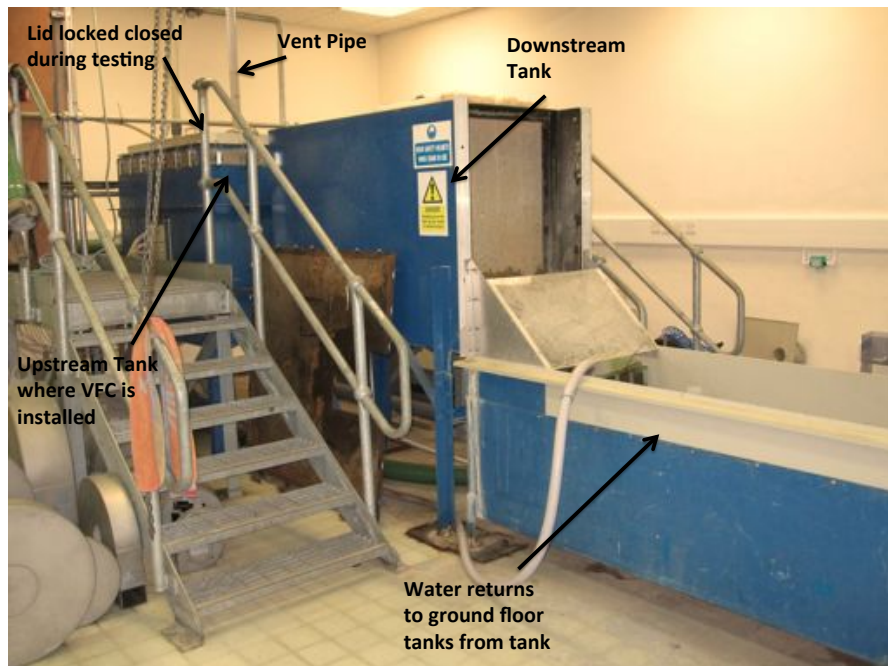


Figure 10: Photograph of First Floor Tanks at Hydro-International Plc. Clevedon Offices

upstream tank where the VFC is installed (Figure 11), the other in the third tank where water returns to the ground floor sum tanks (bottom right of Figure 10). An electromagnetic flowmeter is also connected to the ground floor pump to measure flow rate through the test rig. Maximum water level during testing was limited to the height of the shortest tank since all tanks were vented to atmosphere, and the maximum achievable and measurable flow rate of the facilities is 50 l/s [15].

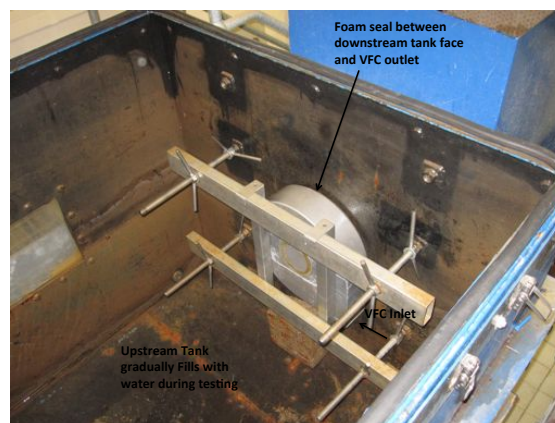


Figure 11: Bolt arrangement for installing VFC for Testing (Control VFC Pictured)

Each VFC under analysis was mounted and bolted into position in the upstream tank, as Figure 11 indicates. A thick piece of water resistant foam was placed between the VFC and the downstream wall of the tank to ensure a tight seal and prevent any leakage during testing. To prevent any leakage from the upstream tank itself during testing, there exists a built-in lid which was securely locked shut for the duration. A vent pipe (to the atmosphere) installed at this lid surface prevented any pressure build up within the system. This vent and the pressure transducer in the tank together ensured no other pressures were present during testing other than the static pressure caused by gravity. The maximum achievable head level was 2m above the VFC invert level, but with the vent pipe installed, additional hydraulic heads up to 0.5m above the physical height of the tank could be tested [15]. Pressure loss through the VFC was then determined by measuring the static pressure difference between the upstream and downstream (centre tank in Figure 10) tanks.

Data logging of the tests was automated via the software LabVIEW 8.3, running on a PC. The flowmeter, head transducers and the pump inverter are all connected to a PROFIBUS (process field bus) network, established by [17] and raw data for head and flow is obtained from the tests in a txt. file format. The pump was programmed to operate with a continually increasing frequency (this increment specified) to vary the flow accordingly.

Within the bracket shown in Figure 11, it was not possible to accurately mount the VFC at the same level for each test. To establish the true VFC datum level, water was pumped into the VFC for a brief period of time and then allowed to drain out of the VFC until it flattened at the outlet invert level. This process also highlighted whether any leaks were present between the downstream wall of the tank and the VFC (the water level would fail to level if there were are leakages).

Test procedure was carried out as follows;

1. Attach/rotate appropriate test plate to the unit securely via bolts in flange (Figure 6)
2. Ensure tank lid securely tied back and safe to enter tank
3. Loosen wing nuts and move brackets (Figure 11) to provide sufficient room to manoeuvre VFC into position
4. Align downstream face of VFC against downstream side of upstream tank, checking outlet is approximately concentric to the outlet pipe
5. Ensure VFC inlet is vertical, check using spirit level
6. Once satisfied with VFC position, securely tighten wing nuts to brace VFC but ensure no obstructions to flow will be caused by the bars around the inlet
7. Close tank lid and lock shut, attach vent pipe
8. Open valve from downstream tanks and initiate pump until VFC is submerged

9. Turn off pump and wait for VFC invert level to be established
10. Program pump frequency range via PC LabVIEW 8.3, switch pump on and begin testing

## 6.2 Test Accuracy and Repeatability

All test instruments were calibrated as part of [15] study, and are continually monitored by the research and development staff at Hydro-International, Clevedon. Pressure and flow rate within the test rig fluctuates during testing as a result of the centrifugal pump and the severity of these fluctuations increases with flow-rate. To minimise the deviations, a moving average smoothing algorithm was applied to pressure and flow rate measurements as they were obtained during testing [15]. All experimental results in Section 7 therefore have this moving average applied to them at the same time data logging occurred.

With regard to test repeatability, as Figure 12 demonstrates, the test facilities at Clevedon produce near identical test results for the same unit. Considering the time limitations allocated for testing and also the length of time taken for each test to complete, it was decided unnecessary to repeat any tests. This in no way however suggests that any findings are not subject to further investigation; it only identifies that repeat testing for the purpose and aims of this study is not necessary to increase test accuracy.

## 7 Results

For the VFC assessments completed as part of this study, readings for pressure and flow rate were programmed to be logged automatically at three second intervals for all tests except for the control unit, which as explained in Section 7.1, was set at an interval 15 seconds. Raw data files for these tests in txt. format are attached in Section 11 (Appendix). Table 5 below gives details of test durations and invert levels for each test completed.

Table 5: Selected Modified VFC Outlet Shapes and Design Descriptions

Order	Test Name	VFC Invert Level (mm)	Test Duration (hrs)
1.	Control	572	2.9
2.	45° Square	559	4.11
3.	Square	575	4.13
4.	Circle	561	2.93
5.	30° Triangle	567	4.31
6.	Triangle	574	4.28

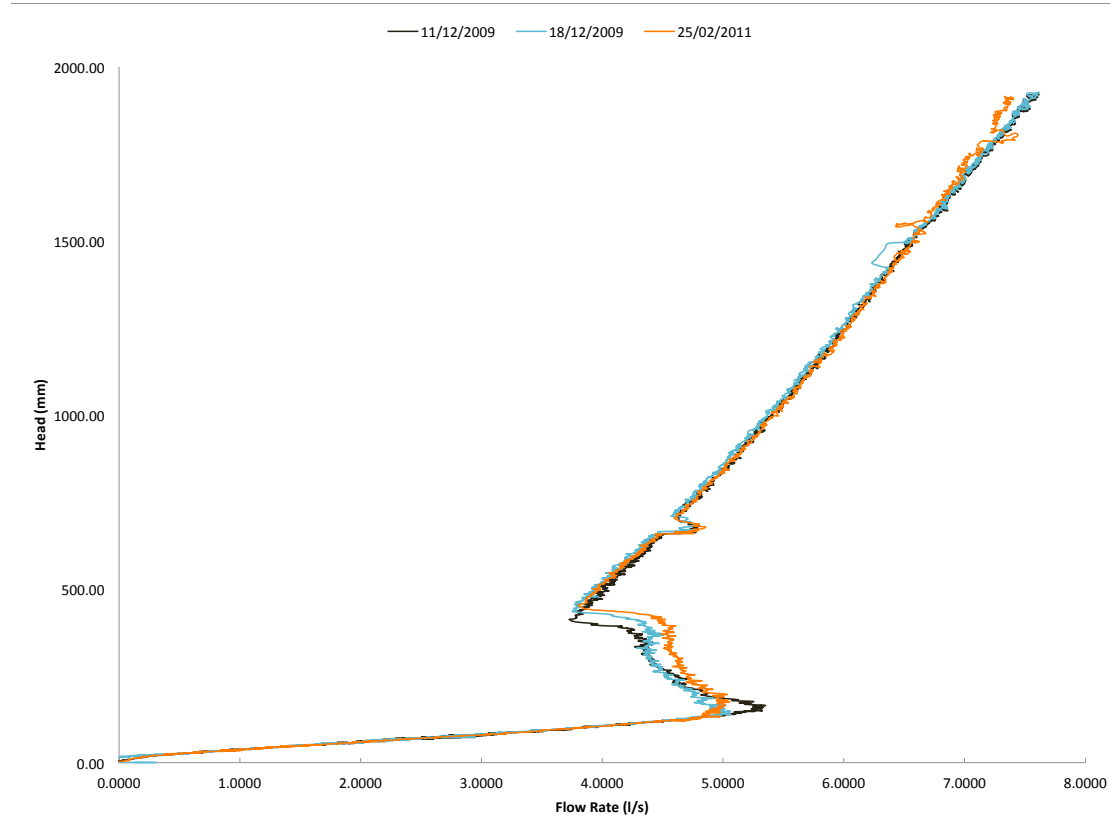


Figure 12: Graph Comparing Results of Three Identical Tests Completed on the same 100mm Cylindrical-Type Unmodified VFC

## 7.1 Control VFC Tests

Figure 12 compares results of three tests carried out at Hydro-International on the same 100mm outlet diameter cylindrical-type VFC. Two tests were carried out by the Research and Development department at the company prior to this project, dated 11/12/2009 and 18/12/2009 respectively. The orange line represents the Control test completed during the six days spent at Clevedon for this project. During the time between these three tests the VFC unit has undergone no modifications and has remained in storage at the Clevedon site.

As Figure 12 highlights, the results before and after the transitional phase are consistent, with the orifice flow stage (heads below approximately 100mm) remaining virtually identical during each test. It should also be noted that the fluctuation present on all test curves between 500mm to 700mm head is a result of the water level in the upstream tank reaching the tank lid. As the water level passed into the vent pipe, the discontinuity within the cross-sectional area caused the head-flow characteristics to fluctuate. It is



not representative of a change in flow regime within the VFC, but a numerical discretion within the moving average algorithms applied to the results within the data-logging software.

For the test dated 18/12/2009, Hydro-International staff advised the graph deviation around the 1500mm head level (rectangular shaped fluctuation) was a result of an accidental tampering of the pump settings during the running of the test, and is not demonstrative of the true head-flow characteristics of the VFC at this stage. The two other tests show no fluctuation at this point which provides redundancy within this statement and highlights the dip as a test error and not a performance anomaly.

It is interesting to observe that whilst all other stages of VFC operation have maintained consistency throughout these three tests, there is a high level of variation within the transitional stage results. This coincides with the work of [15] who during experimental testing of cylindrical-type VFC devices also found significant changes in results within this mode of VFC operation. Since the mechanisms within vortex formation and precession are complex, the array of phenomena occurring may be responsible for unsteadiness and the hysteresis within the results achieved during this phase for identical tests. It is also useful to note that whilst the transitional phase is very varied, the point at which the vortex stabilises (Point C Figure 2) regains reasonable consistency between tests. The reasonable consistency within this point on Figure 12 suggests that regardless of the sporadic flow changes occurring during the transitional phase, the VFC will establish its vortex flow regime at the same point during each use. This is the most important point on the Head-Flow curve for the VFC as it deems when the VFC begins to return back to the design head-flow conditions towards Point A, Figure 2 [13], and ultimately its control capabilities during a storm event. This suggests to design the VFC around Point C since it demonstrates a suitable level of steadiness.

The control test carried out on 25/02/11 would appear to fluctuate slightly within its head-flow curve at head levels between 1500mm and 2000mm compared to the other two control tests. This could be attributed to a discretion within the time increment applied to the control test; since this was the first test completed by the author, pump frequency was increased with an increment time of 15 seconds. Later Hydro-International laboratory staff advised the use of a 3 seconds increment, as from previous experimental work of this nature, this has proven to be the most suitable to apply to tests of this nature. The more turbulent appearance of the control graph in this region may therefore be a result of marginally greater fluctuations within the 15 second average plot against the 3 second average plot. This would also be reasonable to conclude since when comparing the low flow regions of the graph, where flow can be assumed laminar, the curves between tests are near identical. In reality, the differences in increment time does however not produce results that vary significantly, therefore any reasons for concerns between accuracies of the tests are negligible. The main regions of interest on the graph (heads below 1000mm) are identical.

One other factor to consider which may have influenced the control test (25/02/2011)

in Figure 12 compared to the previous tests carried out is that since 2009 Hydro-International have improved their calibration measures at the Clevedon test facilities, thanks to the works of [15]. This could have increased the accuracy of the results obtained in 2011, and therefore may provide better justification to the slight differences in head-flow curves achieved in Figure 12 against the differences in time increments applied. It is unlikely since the tests were completed in the months of December and February that any other external factors such as water temperature would have any impact on the test results.

## 7.2 Modified Outlet Shapes

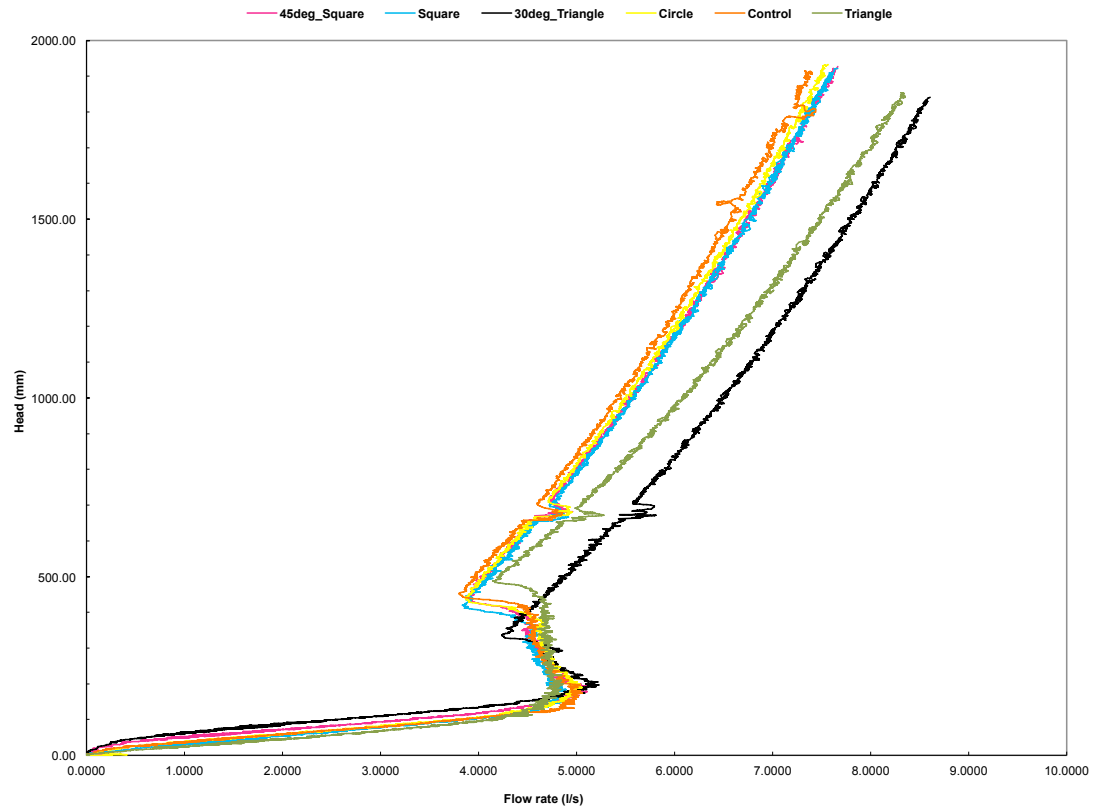


Figure 13: Comparison of head-flow rate curves for all five modified outlet shape designs against control cylindrical-type VFC

As Figure 13 demonstrates, considerable differences were achieved for the various outlet shapes tested. The most significant differences in VFC performance were generated by the triangular outlet plate (in both orientations). These particular results have been highlighted in Figure 15, and are discussed in more detail in Section 7.5 below.

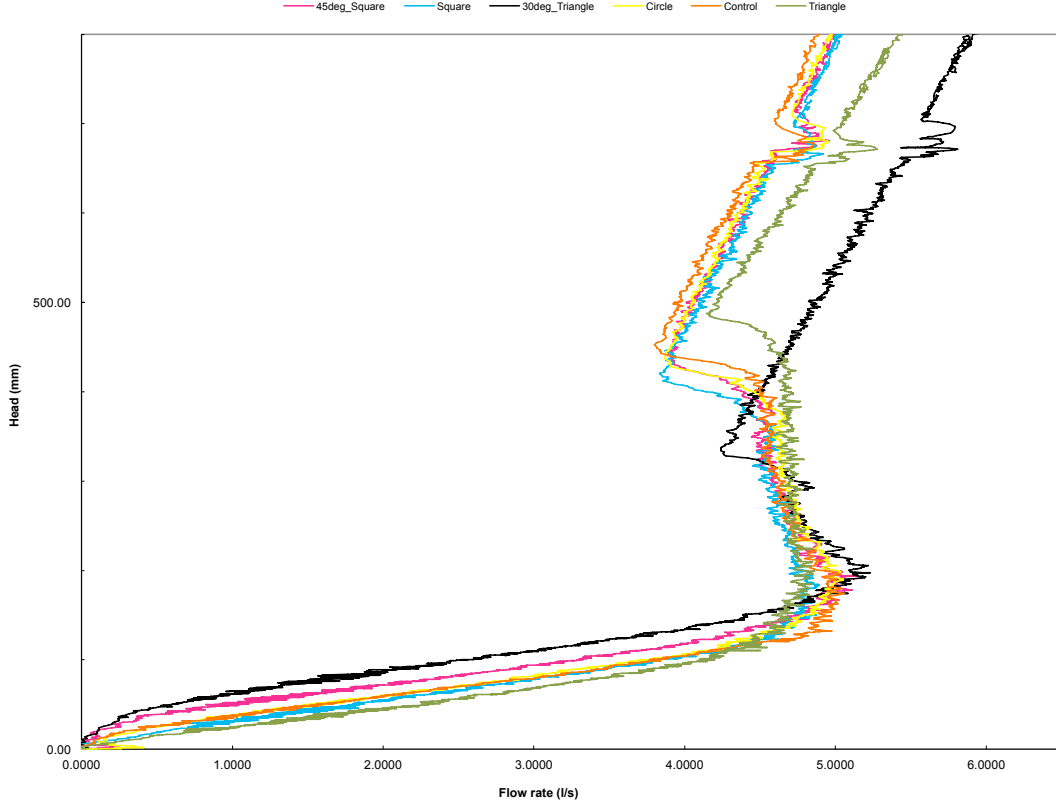


Figure 14: Magnified section of transition zone from Figure 13

### 7.3 Low Flow Rates

Figure 14 gives a focused view of the low-flow section of the Head-Flow graph presented in Figure 13. In the cases of the  $30^\circ$  triangle and  $45^\circ$  square, where the outlet is acting as a vee weir, flow rates recorded are higher than those achieved through the control VFC with its circular outlet. Contrastingly, where the outlet is acting as a rectangular weir during the square and triangle tests, flow rates resemble the control characteristics much more closely, and in the case of the triangle, flow rate during this phase of operation is reduced.

Although the key focus for the design of a VFC is on its ability to reduce outflow during storm events, it is interesting to observe that for the case of the outlet acting as a vee weir, greater outflow occurs during typical low flow scenarios. This may be advantageous for further reduction in upstream storage requirements. Referring back to equation (7) and (8) for the case of the vee weir, the upstream head is more weighted at  $h_2^{\frac{5}{2}}$  against  $h_2^{\frac{3}{2}}$  for the rectangular weir within the ideal flow equations. This gives justification to its increased sensitivity at low flow rates, and also therefore why it would appear to allow

marginally increased flow release at low flow rates.

## 7.4 High Flow Rates

The square plate in both regular (*square*) and  $45^\circ$  orientations did not produce results too dissimilar to the standard cylindrical-type VFC. The transitional phase is slightly shorter for both tests as Figure 14 highlights, and the point at which the vortex initiates (Point B, Figure 2) wavers marginally from that of the control VFC.

As mentioned in Section 1.3 and as Figure 3 of the storm hydrograph highlights, the main aim of any modifications to the VFC is to enhance its flow control capabilities during a storm event, and to maintain a given flow rate against fluctuating heads. In an ideal sense, this would generate a vertical line on Figure 13 after the transitional phase has occurred and once the VFC is in its vortex phase (Mode 4, Table 2). These results therefore suggest that whilst the *square* outlet may stabilise sooner (with a lower kick-back point), this does not generate an overall improvement in the flow control characteristics of the device. Moreover, the vortex initiation point for the square occurs at a lower flow rate than for the control and the  $45^\circ$  *square* outlet, which is again disadvantageous as the point at which the VFC is beginning to have a throttling effect is occurring at a reduced volume of flow, therefore increasing the potential upstream storage requirements within the drainage network.

Since no one truly understands what happens during the transitional phase of the VFC operation, it is difficult to establish with any certainty whether a longer transition is advantageous or disadvantageous in terms of VFC performance. Realistically however, the difference between the kick-back points for the *control* and *square* plate, as Figure 14 highlights, are not significant enough to consider having any serious implications to the performance of the VFC, particularly since once the vortex stage is stabilised the square outlet demonstrates reduced flow control capabilities compared to the control VFC unit.

Another interesting finding from this investigation is the difference in results achieved for the circle outlet and the control VFC tests. Since the outlets can be assumed identical for both tests (excluding the minor manufacturing tolerances) it would be reasonable to expect more closely related results from the two tests. The justification for these discrepancies could be due to significant frictional losses occurring within the prototype VFC compared to the standard VFC (control) unit. It is likely that the flange and irregular connection joints created additional disturbances to flow through the prototype VFC. The results may relate more closely (in line with those achieved in the control comparison graph in Figure 12) if the tests were carried out on a standard VFC unit as the outlets would be truly identical.

This could also suggest that the results for the other outlet shapes are likely to also be subject to frictional losses, and that if these had been incorporated into a standard VFC unit the results may vary slightly. Due to cost constraints within this project

manufacturing five separate units to complete tests in this way was not a feasible option. Most importantly, since all tests under analysis (except the control VFC, but which is directly comparable to the *circle* test) here were completed using the prototype unit, the discrepancies due to frictional losses can be considered constant throughout each test.

## 7.5 Triangular Outlet Results

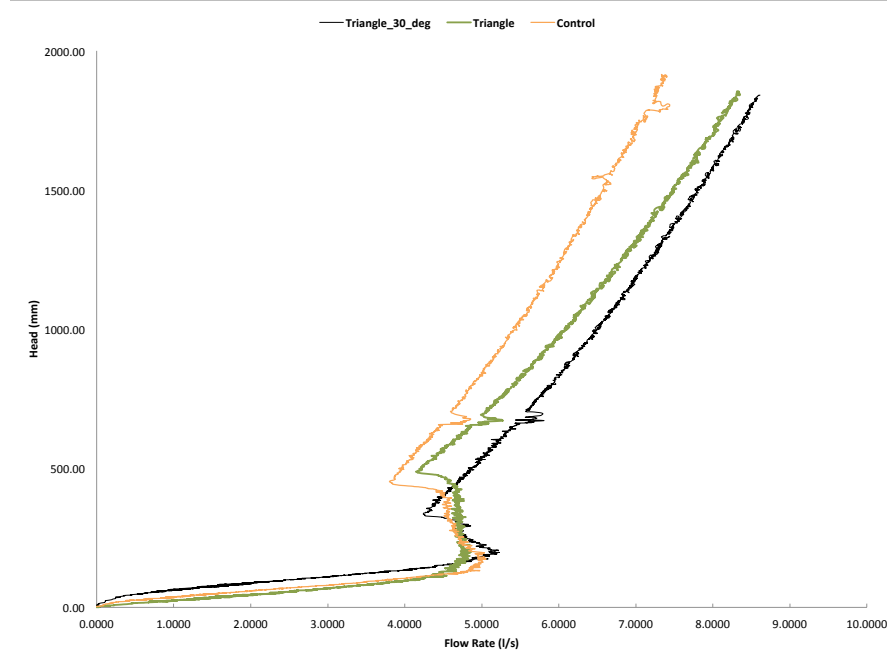


Figure 15: Comparison of head-flow rate curves for triangle shape outlets against control cylindrical-type VFC

A very distinct feature of the triangle outlet is the apparent stability within the transitional phase of the VFC operation, forming a near-vertical line on the Head-Flow graph (Figure 14). From observing the tests in progress in the laboratory at Clevedon, it was clear that as water exited the VFC through the triangle outlet, in both orientations, flow was much more disorderly compared to the control VFC. As can be seen in Figure 16, for the *triangle* case in particular, a constant stream of water outflowed, almost as orifice flow from the bottom of the outlet of the VFC whilst the remaining proportion of flow was exiting heavily down the right hand side of the VFC outlet. This would suggest that the vortex was unable to stabilise fully, allowing a small portion of water entering the VFC to pass through relatively undisturbed.

Flow control for the *triangle* outlet in both orientations is significantly reduced compared to the control curve (the gradient of the curve after the transitional phase is much lower).

In particular for the *triangle* outlet, the graph does not remain linear in this phase of operation (1000mm head and above), but in fact shows an increasing level of flow rate for increased heads.

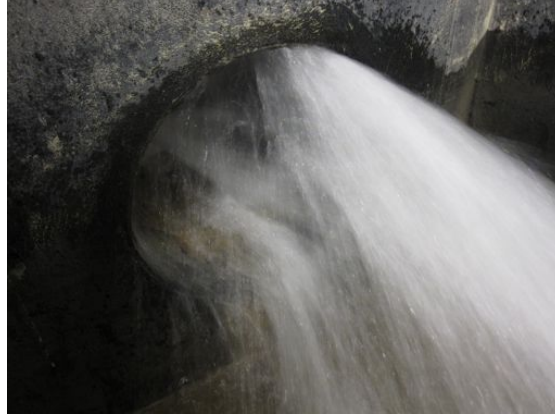


Figure 16: Image of outlet of VFC during testing with triangle outlet installed

Further still, the point at which the vortex begins to form (Point B, Figure 2 for these two outlet shapes is also higher, again suggesting increased volumes of water are able to pass through the VFC with these outlet shapes installed. The kick-back points for both triangular outlet orientations also vary dramatically from the control VFC. For the *triangle*, this test would suggest that the vortex takes much longer to stabilise, and that transition is a more lengthy process. Contrastingly for the *30° deg triangle*, the transitional phase is much shorter and the kick-back occurs much sooner than for the control VFC. Having said this, similar to the *square* and *45° square* tests, the flow control capabilities of the VFC with both orientations of the triangular outlet are reduced, the most significant reduction of all being with the *30° triangle* outlet.

## 7.6 Discharge Coefficient Results

Note: Similar to Figure 13, the fluctuation in the curves on Figure 17 at approximately 7000 H/D are again a result of the water level reaching the top of the upstream tank

Using Equation (6), The Coefficient of discharge ( $C_d$ ) can be calculated;

$$C_d = \frac{Q_{actual}}{A_0 \sqrt{2gh}}$$

Figure 17 shows curves of  $C_d$  against measured head (data logged during tests) divided by outlet diameter for each VFC outlet shape tested. Although  $A_0$  is noted in Section 5.1 as the orifice area, more specifically this is the wetted area of the outlet, which

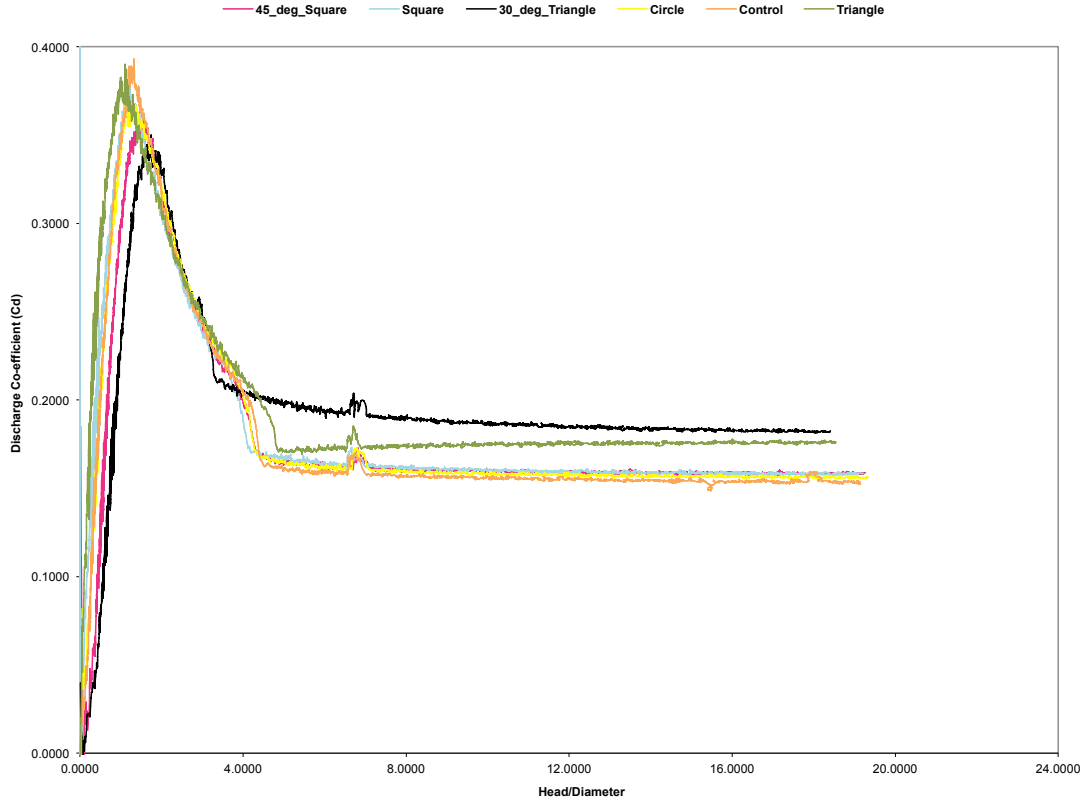


Figure 17: Comparison of discharge coefficient against Head/Diameter curves for all five modified outlet shape designs against control cylindrical-type VFC

during Modes One and Two where open flow and swirling flow conditions are occurring, does not equate to the entire outlet diameter but is proportional to the depth of flow within the VFC. What Figure 17 therefore does not account for is the changes in wetted area during these phases, as within Figure 17 all flow rates are plotted against the full outlet area value. It was not within the scope of this study to attempt to approximate the changes in water depth within the VFC during these phases and to analyse the discharge coefficient of the device accordingly since these low flow rates have little influence on the throttling capabilities of the VFC during a storm event. Figure 17 merely provides an indication of the changes to the discharge coefficient through the VFC assuming water level remains above the VFC soffit for all flow rates.

The purpose of plotting  $C_d$  against Head/Diameter ( $H/D$ ) instead of Head alone has been to compute a non-dimensional comparison between units of different scales or design. A direct comparison of the changes in discharge characteristics can therefore be observed from this graph, regardless of VFC unit geometries. Whilst the outlet hydraulic diameters have remained constant during this test (cross-sectional area of outlet

has been maintained) plotting the curves without any geometric constraints allows for comparison between other VFC units outside this project if the results were to be used for any additional purposes by Hydro-International.

In figure 17, during the orifice stage of flow and whilst swirling flow is induced, the discharge coefficient shows a steady increase corresponding to the gradual increase in flow through the VFC provided by the automated pump. Once transition initiates, energy losses within the VFC significantly increase, reducing the flow rate through the device, and this is represented by the sudden decrease in the value of the discharge coefficient. Due to the highly turbulent nature of the flow, the graph shows a degree of fluctuation. As demonstrated by Figure 13, the transitional phase is very unstable and it is therefore unsurprising to observe this instability within the discharge coefficient values also. Eventually once the vortex has stabilised, the discharge coefficient also stabilises. This indicates that the level of discharge is remaining relatively constant with increasing head, and that energy losses within the VFC have also stabilised, as Figure 13 also shows.

What is of particular interest within Figure 17 is that the triangular outlet plates show less stability (the curve deviates more from the horizontal compared to the control curve on the graph at  $H/D \geq 8000$ ) and settle at a higher average discharge coefficient. This again implies that the flow control capabilities are less for the VFC with both the triangular outlets, but most severely so for the  $30^\circ$  triangle case. It would again highlight that greater energy losses are occurring within the flow and the vortex regime is not establishing effectively enough as required in order to prevent flow fluctuations with head fluctuations.

## 7.7 Theoretical Comparisons

The concept of a two-celled vortex is one which many researchers have previously concluded, and a model which is becoming increasingly accepted for vortex flow typical of that induced in a VFC. The previous work of [15] and [16] highlight that within this type of closed vortex flow, a two-celled vortex exists with an air core surrounded by a region of slower rotational flow. As Figure 13 demonstrates, all tests on the modified VFC operate in-line with these findings and this model, with clear regions of open flow, a transitional phase and development of an air core and a vortex phase all occurring.

In [14], the formation of this air core from the free surface is linked to the pressure difference induced across the flow as a result of swirl. Time restraints for this project have not allowed for investigation into these pressure changes occurring, however the work of [9] gives an indication of this aspect of the flow regimes and effects on the vortex core according to CFD modelling of the experiments.

It is also noted in [14] that as flow continues to increase and develop, this inner vortex cell eventually detaches from the bottom boundary layer of flow, and air is gradually expelled entirely from the flow regime. For the *triangle* outlet case, since the transitional



zone demonstrates much more stability and occurred more gradually, it would suggest that this air entrapped within the VFC is being drawn out at a more constant and gradual rate compared to the control VFC or indeed any of the other outlet shapes tested. When considering the shape of a triangle (Figure 18), this would seem logical as there is a narrow void above the incircle area in which the vortex is able to form, allowing air to escape more readily. In line with this, the sudden kick-back present in Figure 15 could be a result of the last of the air suddenly being removed through the tip of the triangle of the VFC outlet to form a full vortex once the flow is fully established and the VFC outlet fully submerged.

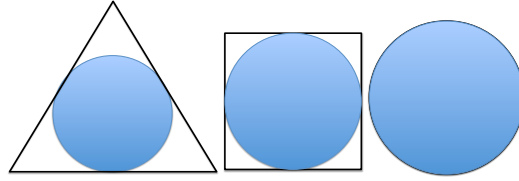


Figure 18: Sketch of incircle areas for each outlet shape (not to scale)

It is reasonable to assume based on observations made during testing, that regardless of the shape of the outlet the core will form approximately as a spherical core due to the helical nature of the fluid motion. What is therefore of most interest within these results is that although the outlet cross-sectional area is maintained throughout all shapes tested, the effective area in which the vortex can form is compromised, most significantly so in the triangular outlet. Figure 18 gives a very crude representation of the maximum available area in which the vortex core is able to form.

Within an equilateral triangle with sides of length ( $S$ ), the radius ( $r$ ) of the largest incircle able to form, assuming the sides are tangents to the circle, is [19]

$$r = \frac{S}{2\sqrt{3}} \quad (16)$$

Using the dimensions of the shapes given in table 3, it is estimated that for the triangle outlet, the maximum diameter is reduced to approximately 78% of the diameter of a circular outlet of equivalent cross-sectional area.

$$\text{Diameter of Circle (mm)} = 2\left[\frac{134.6}{2\sqrt{3}}\right] = 77.7 \quad (17)$$

This reduction of area in which the vortex core is able to form and precess within the triangular therefore also provides a reasonable explanation as to why the flow control capabilities are so greatly reduced since a smaller and weaker vortex regime is induced. Further still, the vortex initiated does not occupy the full outlet area, which leaves regions where flow is not sufficiently choked and able to pass through the outlet undisturbed (as Figure 16 demonstrates). This links very closely to the findings of [3], who concluded

that the presence of an air core within the flow reduces the cross-sectional area available for water flow; for the triangle outlets, with a reduced core size greater volumes of flow are able to pass undisturbed. To a less severe degree, this also happens within the  $45^\circ$  square and the square outlets, and again provides a reasonable explanation for the reduction in flow control capabilities with these outlet shapes implemented.

## 7.8 Vortex Core Radius

The authors of [11] established that for a given tangential velocity and average velocity at the outlet of the vortex tube, the vortex core radius will adjust so that flow is maximised for a given pressure difference. This implies that the formation of this vortex core is heavily dependent upon the level of tangential or axial flow dominating the flow regime. Since it was not possible to utilise Particle Image Velocimetry or any other form of flow imaging to gauge approximate sizes of the vortex core during testing, the model provided by [3], which [11] later developed, provide a suitable point for discussion on the changes occurring to the magnitude of the vortex core.

Referring back to equation 15

$$R_{cx} = \frac{0.0219 (v_{\theta CS}/v_x)^{-0.686} + 1}{0.700 (v_{\theta CS}/v_x)^{-0.686} + 1}$$

Using this equation, if the components of tangential velocity are known, perhaps determined using CFD, values of the core radius for each outlet could be approximated. From the experiments carried out as part of this study, and in line with the findings of [3], there is reason to suggest that flow control capabilities of the VFC are significantly influenced by the area in which the vortex is able to form and expel air through. Combining Equation 15 with these findings, it would be logical to propose the potential for a model which relates the efficiency of the VFC in terms of its head-flow characteristics to the magnitude of the core of the vortex and/or to the physical cross-sectional area of the outlet in which the vortex can form. A ratio of device efficiency to outlet incircle area would appear to exist, and with further investigation there is the potential for development of a model relating these two performance factors.

## 8 Conclusions

Referring to the deliverables outlined in Section 1.4, all five key aims of this study have been achieved, and reasonable conclusions relative to theory and previous studies have been formulated on the effect of a modified outlet shape to VFC design.

With regard to overall improvement to the operation of a VFC, the modified outlet shapes tested in this study have not been found to have a positive impact. The square and triangle outlet shapes in two respective orientations were all found to reduce the

flow control against fluctuating head capabilities of the VFC compared to a standard cylindrical-type VFC unit. This has been considered as a result of a reduction in the available outlet area in which the vortex core is able to form and expel air downstream. With a more constricting outlet shape, the vortex regime failed to stabilise as sufficiently as within the cylindrical-type VFC unit. With less of the outlet area occupied by the vortex (and its air-filled core) and a smaller, therefore weaker, vortex induced, greater volumes of flow were able to pass through the VFC.

Some positive findings within the triangle outlet shape were however discovered, as the transitional phase between swirling flow and vortex flow appeared to stabilise significantly for this outlet shape. Having said this, both this study and the work of [15] conclude that the transitional zone is subject to hysteresis, therefore one test alone on this outlet shape is not sufficient to conclude this improvement with any certainty. More importantly, whilst the triangle outlet may appear to remain more stable in transition, it has very poor flow control capabilities compared to the standard VFC unit and therefore in its current design should not be considered for use within a VFC device.

Further still, introducing an outlet shape with sharp edges and corners increases the risk of blockages within the VFC. Whilst these edges could be rounded, as this study has highlighted through the use of a prototype unit with obscure edges, this could may have implications for the operational characteristics of the VFC due to changes in frictional losses. Regardless, any edges would fail to reach the effectiveness of a circular outlet at reducing blockages and allowing free and safe passage of wildlife. Since this is an aspect of the VFC ethos highly important and desirable to its use within Sustainable Drainage Systems, as it reduces the level of maintenance required to the VFC the operation, and increases its environmental suitability, this problem poses another argument against any changes to the outlet design.

## 8.1 Further Work

Recommendations for further work are as follows;

1. To firstly verify any of the conclusions drawn from this study, repeat tests should be completed for all outlet shapes of interest. This is considered to be particularly necessary since as Figure 12 demonstrates, VFC transitional characteristics are unstable and may therefore alter during a repeat test. It would also be most worthwhile to incorporate these modifications into a standard cylindrical-type VFC unit to eliminate the frictional losses occurring between the detachable plate and flange section of the prototype unit tested in this study. This would provide results more representative of the true impact of the modifications.
2. To investigate the impact on performance of a modified triangular outlet. By implementing an isosceles triangle instead of an equilateral triangle, the incircle area of the outlet could be increased to enhance the flow control capabilities of the outlet shape, and the tip of the triangle also elongated to enhance the gradual

release of air through the VFC. Care would however need to be taken to ensure the inlet to outlet ratio was maintained, otherwise undesired effects to the VFC performance may also occur as a result of the disruption to this ratio.

3. Considering the flow-control capabilities of the VFC are known to be a function of the Area of the Outlet, the Reynolds Number of the flow and the Discharge Coefficient from this study, investigate more thoroughly the potential of modelling the ratio of incircle area within the outlet area to the head-flow efficiency of the device.
4. Analyse the impact of axisymmetric outlet designs in the VFC, particularly since much of the literature collated as part of this study suggests axisymmetric designs to have considerable impact over vortex flow functionality. Whilst the outlet shapes studied here produced interesting findings, axisymmetric shapes may offer alternative results which could provide further information over the key factors which influence VFC operational characteristics.
5. Investigate some of the other modification options to the VFC which were listed in Section 4.2, in particular the inlet area to outlet area ratio, as this would appear to have significant influence over the operation of the VFC

## 9 Acknowledgements

Many thanks to my supervisor Dr Gavin Tabor for continued guidance throughout this project, and to Daniel Jarman and staff at the Research and Development Department at Hydro-International for your patience and help. Thank you also for your generous use of the Clevedon laboratory for these tests.

## 10 Bibliography

### References

- [1] Alekseenko, S. V., Kuibin, P. A., and Okulov, V. L.; (2007) *Theory of Concentrated Vortices; An Introduction* Chapter 3, Springer
- [2] Andersen, A; Bohr, T; Stenum, B; Juul Rasmussen, J; Lautrup, B.; (2003) *Anatomy of a Bathtub Vortex* Physical Review Letters 91, Number 10. The American Physical Society
- [3] Binnie, A. M; Hookings, G. A (1948) *Laboratory Experiments on Whirlpools* Proceedings of the Royal Society of London. Series A, Mathematical and Physical Sciences, 194(1038) pp 398415
- [4] Burgers, J. M. (1948) *A mathematical model illustrating the theory of turbulence* Advances in Applied Mechanics, 1:197199
- [5] Chadwick, A.; Morfett, J.; Borthwick, M.; (2004) *Hydraulics in Civil and Environmental Engineering* Ed. 4, Chapters 4, 5 and 10. Spon Press, London
- [6] Douglas, J. F; Gasiorek, J. M; Swaffield, J. A.; (2001) *Fluid Mechanics* Ed. 4, pp 170–171, pp 202–210, pp 246–251. Pearson, London
- [7] Drainstore  
<http://www.drainstore.com/jfc-hydro-valve-vortex-flow-control-i601906.html>  
Company Website Accessed 04/2011
- [8] European Environment Agency, <http://www.eea.europa.eu>  
Information on European Climate Change Accessed 04/2011
- [9] Engel, B.; (2011) *Evolutions of Vortex Flow Control Design at High Flow Rates* Individual Project, University of Exeter
- [10] Gupta, A. K., Lilley, D. G., and Syred, N. (1984). *Swirl Flows* Energy and Engineering Science Series, Abacus Press
- [11] Hoffmann, A.C., Stein, L.E., (2008) *Gas Cyclones and Swirl Tubes: Principles, Design, and Operation* Second Ed. Springer
- [12] Hydro International Plc  
<http://www.hydro-international.biz/stormwater/floodcontrol.php>  
Company Website Accessed 04/2011
- [13] Hydro International Plc  
*100mm Type STH-L2Z Hydro-Brake Flow Control* HBFC Design, Version 3.6.4 of Technical Specification Criteria and Design Advice  
Accessed 03/2011

- [14] Huang, S-L; Chen, H-C; Chu, C-C; Chang, C-C. (2008) *The transition process of a swirling vortex generated in a rotating tank* Exp Fluids 45: pp 267-282
- [15] Jarman, D.S. (2011) *A Study of the Design of Cylindrical Vortex Flow Controls for use in Urban Drainage Systems* Doctor of Philosophy in Engineering, Chapters 2, 3 and 7. University of Exeter
- [16] Kulkarni, A. A; Ranade, V. V; Rajeev, R.; Koganti, S. B (2007) *Pressure drop across vortex diodes: Experiments and design guidelines* Chemical Engineering Science 64 (2009) pp 1285–1292. ELSEVIER
- [17] LeCornu, J. P. and Faram, M. G. (2006) *Evolving methods for the calibration of flow controls for stormwater and wastewater management* CIWEM 4th Annual Conference, Newcastle, England, The Chartered Institution of Water and Environmental Management
- [18] LeCornu, J. P., Faram, M. G., Jarman, D. S., and Andoh, R. Y. G. (2008). *Physical characterisation and hydrograph response modelling of vortex flow controls* 11th International Conference on Urban Drainage, Edinburgh, Scotland
- [19] Page, J.; (2009) Information on triangle incircles  
<http://www.mathopenref.com/triangleincircle.html> Accessed April 2011
- [20] Nahas, A.; Calvo, A.; Piva, M.; (2010) *Swirling Flow in a Fixed Container: Generation and Attenuation of a Vortex Column* Journal of Fluids Engineering, Vol 132, Issue 11 pp 111204 1–9
- [21] Oetiker, T., Partl, H., Hyna, I., Schlegl, E.; (2011) *The Not So Short Introduction to L<sup>A</sup>T<sub>E</sub>X2 $\epsilon$*  Version 5.01  
<http://ctan.sqsol.co.uk/info/lshort/english/lshort.pdf>, Accessed April 2011
- [22] Stahre, P.; Urbonas, B.; (1990) *STORMWATER DETENTION For Drainage, Water Quality and CSO Management* Chapters 1, 11 13. Prentice-Hall, Inc., New Jersey, USA
- [23] Sullivan, R. D. (1959) *A two-cell vortex solution of the Navier-Stokes equations* Journal of Aerospace Science, 26:767768.
- [24] UK Government, DEFRA  
<http://www.defra.gov.uk/environment/flooding/policy/fwmb/key-areas.htm>.  
Information on the Flood and Water Management Act 2010  
Accessed 05/2011

## 11 Appendix

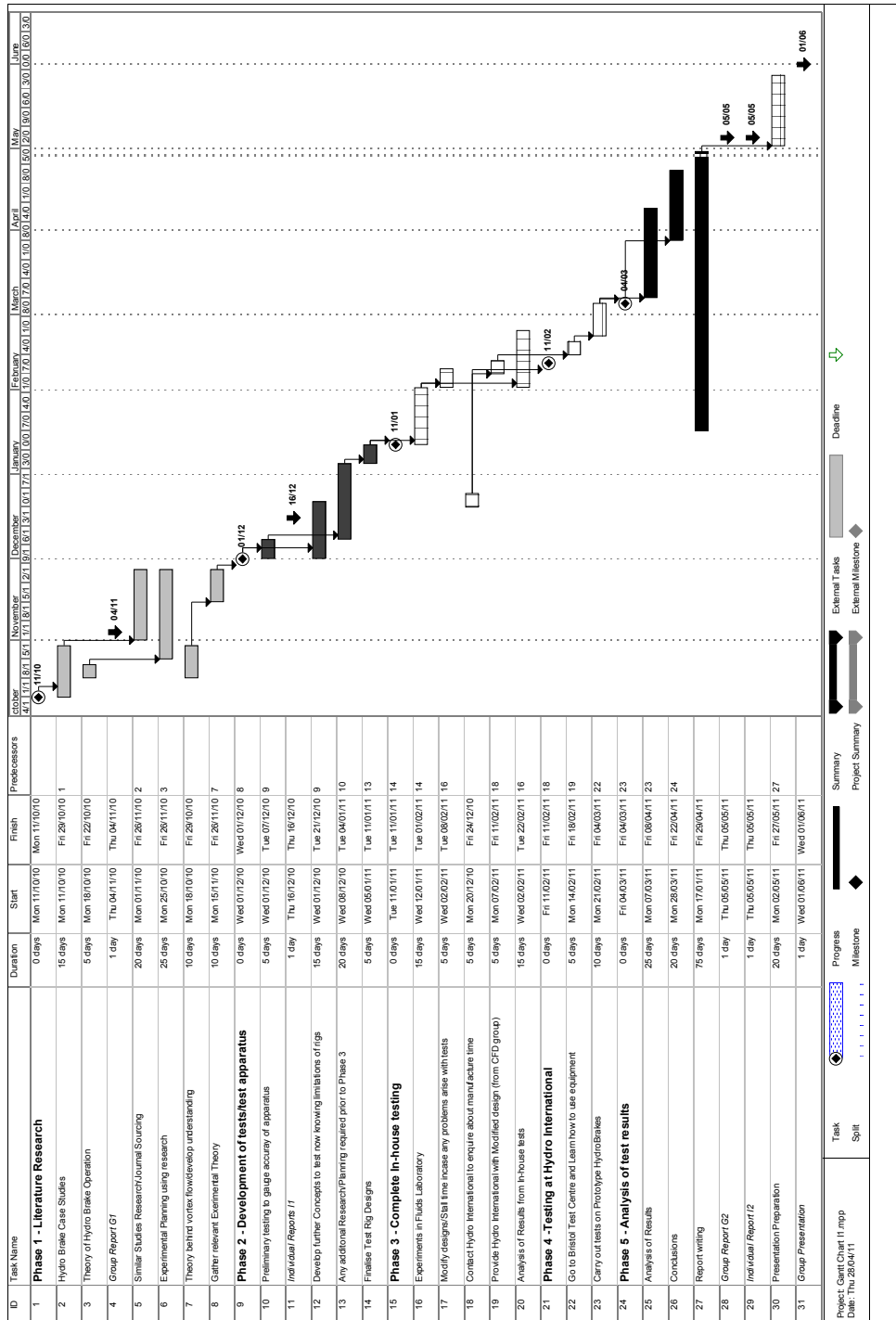


Figure 19: Individual Project Gantt Chart



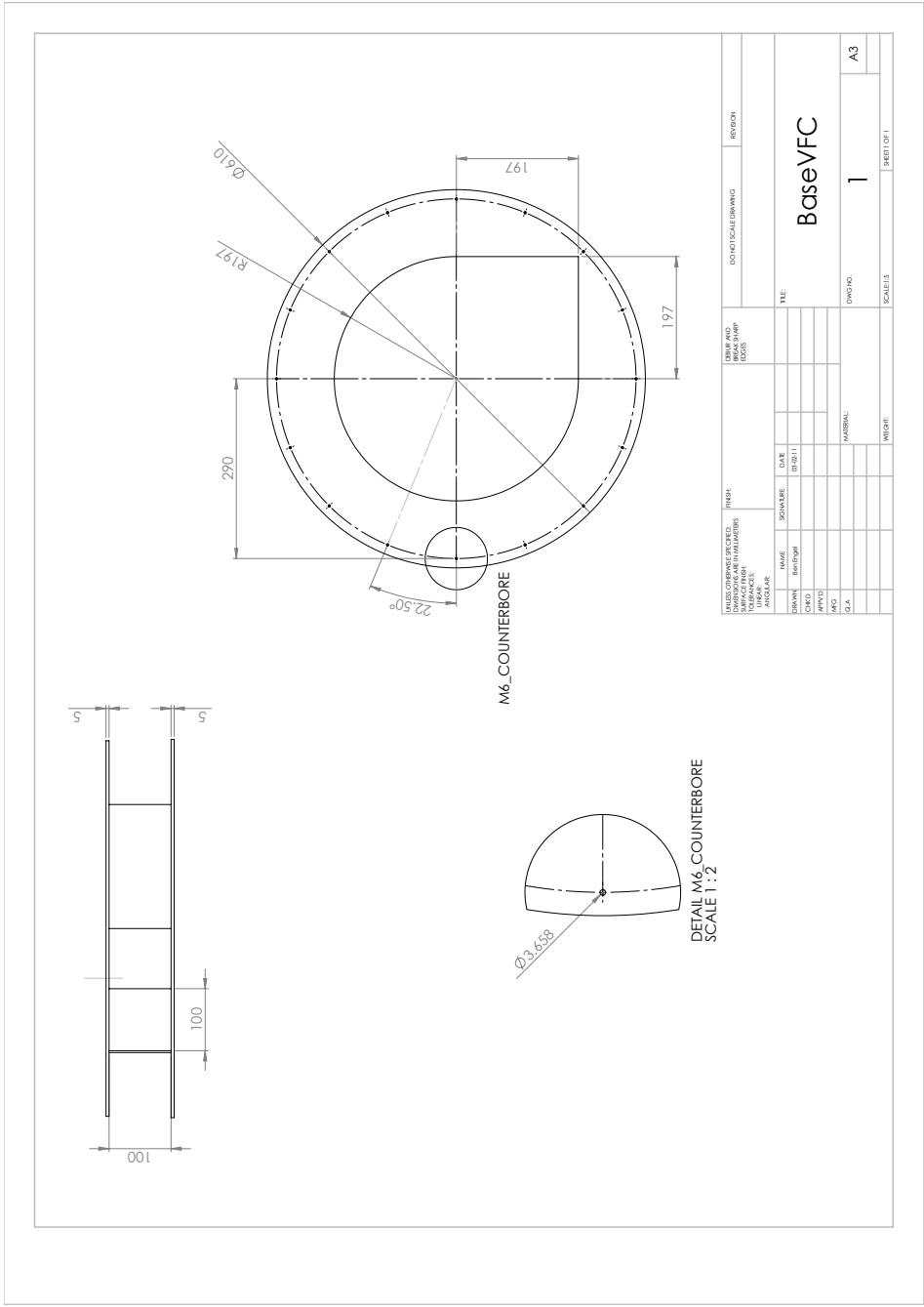
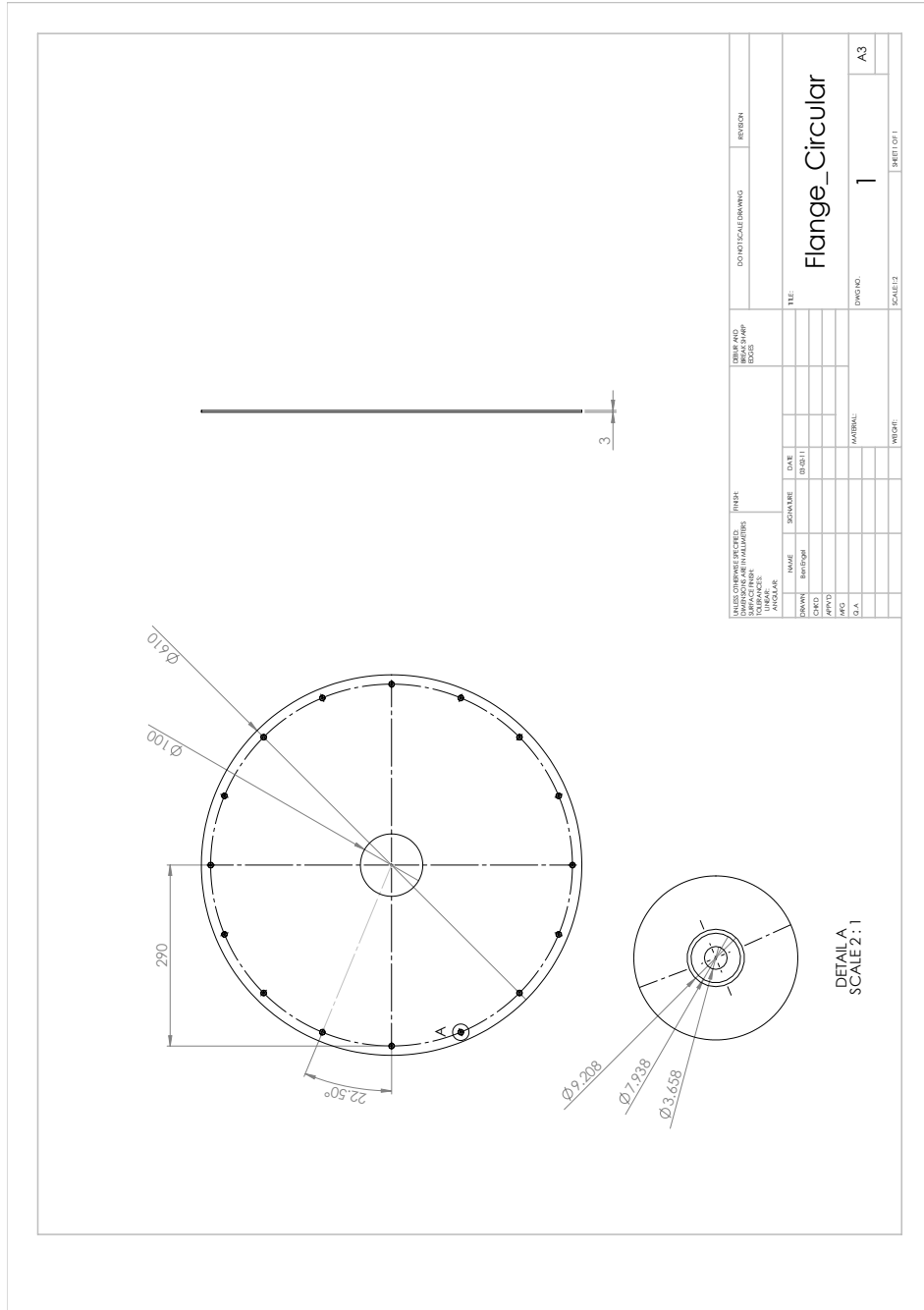


Figure 20: Technical Drawing of Prototype VFC Unit for Testing at Clevedon [9]



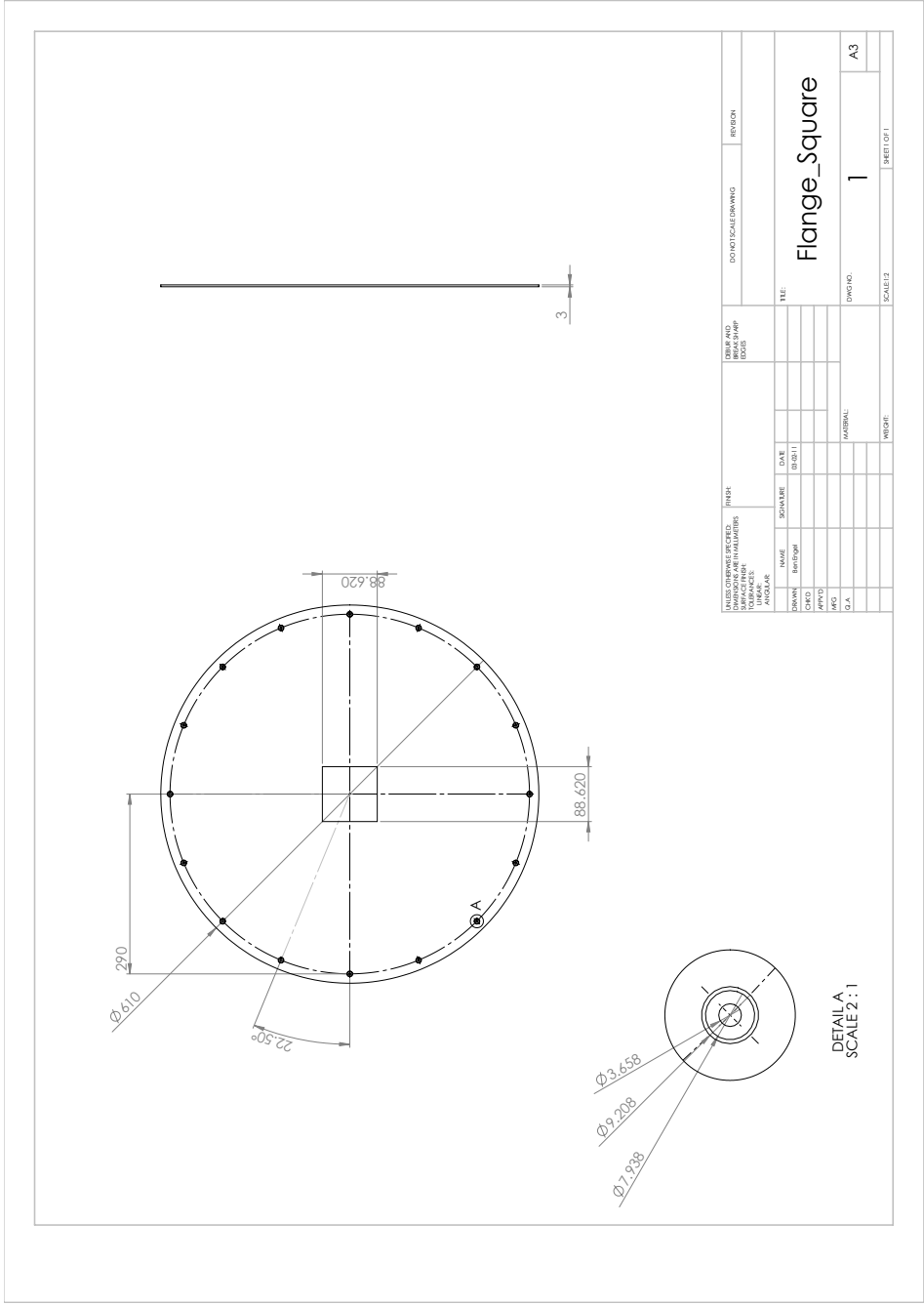


Figure 22: Technical Drawing of Prototype VFC Square Plate [9]

